Electrochemical, surface and computational studies on the inhibition performance of some newly synthesized 8-hydroxyquinoline derivatives containing benzimidazole moiety against the corrosion of carbon steel in phosphoric acid environment

Mohamed El Faydy, Brahim Lakhrissi, Charafeddine Jama, Abdelkader Zarrouk, Lukman Olasunkanmi, Eno Ebenso, Fouad Bentiss

Electrochemical, surface and computational studies on the inhibition performance of some newly synthesized 8-hydroxyquinoline derivatives containing benzimidazole moiety against the corrosion of carbon steel in phosphoric acid environment

M. El Faydy [a], B. Lakhrissi [a], C. Jama [b], A. Zarrouk [c], L.O. Olasunkanmi [d,e], E.E. Ebenso [d,e], F. Bentiss [b,f,*]

[a] *Laboratory of Agricultural Resources, Polymer and Process Engineering, Ibn Tofail University, Department of chemistry, B.P. 133, Kenitra, Morocco*
[b] *Univ. Lille, CNRS, INRA, ENSCL, UMR 8207, - UMET - Unité Matériaux et Transformations, F-59000 Lille, France*
[c] *Laboratory of Materials, Nanotechnology and Environment, Faculty of Sciences, Mohammed V University, Av. Ibn Battouta, PO Box 1014 Agdal-Rabat, Morocco*
[d] *Department of Chemistry, School of Chemical and Physical Sciences, Faculty of Natural and Agricultural Sciences, North-West University, Private BagX2046, Mmabatho 2735, South Africa*
[e] *Material Science Innovation & Modelling (MaSIM) Research Focus Area, Faculty of Natural and Agricultural Sciences, North-West University, Private Bag X2046, Mmabatho 2735, South Africa*
[f] *Laboratory of Catalysis and Corrosion of Materials, Faculty of Sciences, Chouaib Doukkali University, PO Box 20, M-24000 El Jadida, Morocco*

* Corresponding authors.
E-mail address: fbentiss@gmail.com

ABSTRACT

Four new 8-hydroxyquinoline derivatives, namely 5-((1H-benzimidazol-2-yl)methyl)quinolin-8-ol (BIMQ), 5-((5-methyl-1H-benzimidazol-2-yl)methyl)quinolin-8-ol (MBMQ), 5-((5-chloro-1H-benzimidazol-2-yl)methyl)quinolin-8-ol (CBMQ) and 5-((5,6-dichloro-1H-benzimidazol-2-yl)methyl)quinolin-8-ol (DCBMQ) were prepared in moderate to good yields through the condensation of 5-(carboxymethyl)-8-hydroxyquinoline and substituted o-phenylenediamine. ^{1}H, ^{13}C NMR and Elemental analysis confirm the formation of the desired compounds. The anti-corrosive potential of these heterocyclic compounds has been studied on carbon steel in 2 M phosphoric acid (H_3PO_4) electrolyte by means of electrochemical measurements. The inhibition efficiency of these heterocyclic compounds was strongly linked to the concentration and the structure of the molecules; reached a maximum of 94.7% for DCBMQ at 10^{-3} M. Data generated from potentiodynamic revealed that the investigated 8-hydroxyquinoline derivatives are mixed type inhibitors. The influence of temperature on the corrosion behaviour was assessed. The four quinoline derivatives adsorbed according to the Langmuir's adsorption isotherm. Surface analysis (SEM and XPS) confirmed the formation of a protective layer adsorbed on the steel surface. DFT calculations suggested that 8-hydroxyquinoline derivatives adsorb on the metal via the 8-hydroxyquinoline ring and their corrosion inhibition potential have some linear correlation with the degree of co-planarity of the benzimidazole and hydroxyquinoline rings. Monte Carlo simulations showed that the molecules adsorbed on Fe(110) surface through the 8-hydroxyquinoline in a near-flat mode and the adsorption energies both in the absence and presence of aqueous phosphate ions agree with the observed trends of inhibition efficiencies.

Keywords: 8-Hydroxyquinoline; Carbon steel; Phosphoric acid; Corrosion inhibition, EIS, XPS, Theoretical calculations.

1. Introduction

Carbon steel is by definition an alloy of iron that operates under various conditions in several industries where aqueous media, especially acids, are inevitably utilized for different advantageous purposes [1-3]. Hence, corrosion of carbon steel in acidic solution notably with regard to the use of organic inhibitors is a pioneering technical in the field of corrosion science [4-6]. In this context, several reviews about various types of organic inhibitors have been previously documented [7-16]. However, the existing data show that the more efficient organic compounds are suitable to contain heteroatoms such as nitrogen, sulphur, oxygen and also other parameters such as unsaturated bonds and plane conjugated systems comprising any kinds of aromatic rings [17-19]. Moreover, the organic inhibitors act by adsorption on the metal surface and the latter depends on the nature of the surface charge of metal, the allocation of charge on the entire inhibitor molecule [20].

Phosphoric acid (H_3PO_4) is largely used in several industrial sectors such as removal of oxide film, chemical and electrolytic polishing... In other words, phosphoric acid is known by its strong corrosiveness on iron-based materials, hence the need to protect or to limit the attack of metallic materials. However, little works have been done on the corrosion inhibition of steel in H_3PO_4 solution using organic molecules [21-34].

Quinoline derivatives are first actives ingredients in the anti-malarial drugs and have particular biological properties and who poses no significant risk to environment [34-36]. However, the literature uncovers that information with respect to the utilization of 8-hydroxyquinoline and its derivatives as corrosion inhibitor for steel in H_3PO_4 are extremely rare. To the best of our knowledge, 8-hydroxyquinoline and its derivatives have never been used as corrosion inhibitors for steel in H_3PO_4. In this context, the target of this work is to assess the anti-corrosive capability of newly synthesized 8-hydroxyquinoline derivatives, namely, 5-((1H-benzimidazol-2-yl)methyl)quinolin-8-ol (BIMQ), 5-((5-methyl-1H-

benzimidazol-2-yl)methyl)quinolin-8-ol (MBMQ), 5-((5-chloro-1H-benzimidazol-2-yl)methyl)quinolin-8-ol (CBMQ) and 5-((5,6-dichloro-1H-benzimidazol-2-yl)methyl)quinolin-8-ol (DCBMQ) each representing two aromatic rings, 8-hydroxyquinoline ring fused to a heterocyclic (benzimidazol) ring on carbon steel in 2 M H_3PO_4 by means potentiodynamic polarization, and electrochemical impedance spectroscopy (EIS), scanning electron microscopy (SEM) and X-ray photoelectron spectroscopy (XPS) techniques. Theoretical density functional theory (DFT) calculations and Monte Carlo simulations were likewise performed on 8-hydroxyquinoline derivatives so as to associate the corrosion inhibition capacity with their molecular structures.

2. Experimental

2.1. Inhibitors

2.1.1. General informations

All reagents and solvents are imported from Sigma-Aldrich. The kinetics of the reactions were examined by TLC. Melting points were defined through Fargo MP-2D. Flash column chromatography was carried out together with silica gel (0.040-0.063 mm) by elution with hexane–acetone mixture. NMR spectra have been made by Bruker 300 WB spectrometer. C, H, N analyses were realized using a Perkin-Elmer Model 2400 CHNS/O Series.

2.1.2. Chemical synthesis

The synthesis procedure of four kinds of 8-hydroxyquinoline derivatives containing benzimidazole moiety is described in Scheme 1. First, 8-hydroxyquinoline was converted to 5-chloromethyl-8-hydroxyquinoline hydrochloride as described by Burckhalter [37]; the 5-chloromethylquinolin-8-ol hydrochloride was transformed to 5-cyanomethyl-8-

hydroxyquinoline (2) thereafter. [38]. The acid hydrolysis of 5-cyanomethyl-8-hydroxyquinoline (2) leads to 5-(carboxymethyl)-8-hydroxyquinoline hydrochloride (3) [39], which was condensed with 4,5-substituted derivatives of o-phenylenediamine (4a-d) in HCl solution (37 %) to give the desired hydroxyquinolines compounds (**5a-d**).

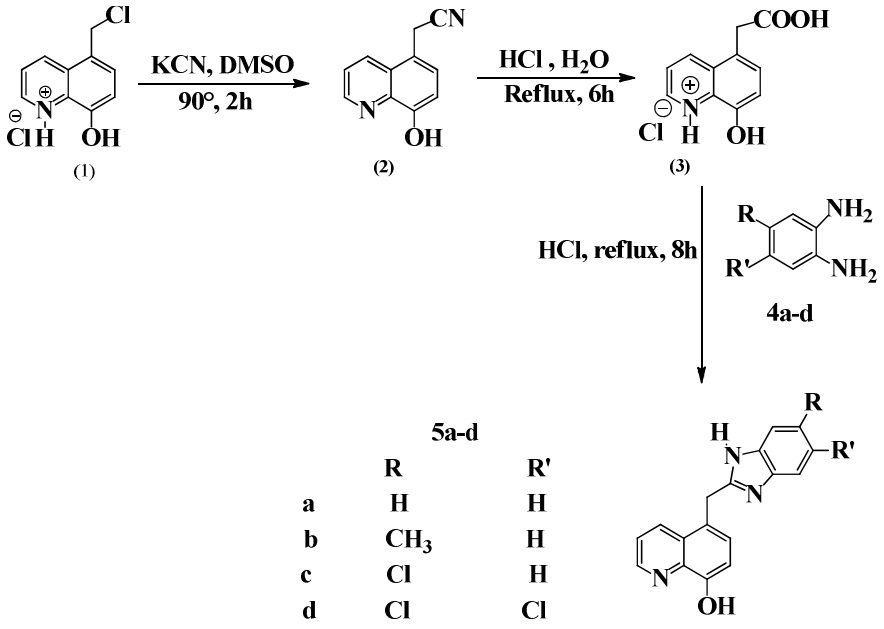

Scheme 1. Synthesis of 8-hydroxyquinoline derivatives containing benzimidazole moiety.

So, the general procedure for the synthesis of 8-hydroxyquinoline derivatives containing a benzimidazole moiety (**5a-d**) has been developed as follows; an equimolar mixture of 4-substituted derivative of o-Phenylenediamine (**4a-d**), 5-(carboxymethyl)-8-hydroxyquinolin hydrochloride (**3**) was refluxed in 4 N HCl for 8 h, after cooling, the precipitate was obtained after addition of aqueous sodium hydroxide, the separated product was purified through Flash column chromatography. The structures of 8-hydroxyquinoline derivatives were identified by NMR and elemental analysis and their spectra are attached in supplementary data. Spectral and analytical data of synthesized 8-hydroxyquinoline derivatives containing a benzimidazole moiety are summarised in Table 1.

Table 1

Abbreviation, molecular structure, spectral and analytical data of synthesized 8-hydroxyquinoline derivatives containing a benzimidazole moiety.

Compound	Abbreviation	Structure	Spectral and analytical data
5a	**BIMQ**	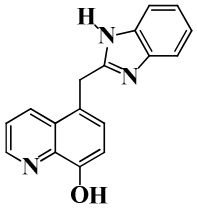	Yield 60 %, M.P. 206 °C, brown of solid. ^{1}H NMR (300 MHz, Me_2SO-d6), δppm = 5.0 (s, 2H, -CH_2-); 7.0-8.89 (m, 9H_{arm}); 12.15 (1s, 1H, NH). ^{13}C NMR (300 MHz, Me_2SO-d6), δppm = 37,18(HQ-CH_2-benzimidazole); 111.32-152.74 (CH_{arm} and C_{arm}). Elemental analysis for $C_{17}H_{13}N_3O$: calcd.: C, 74.17; H, 4.76; N, 15.26; Found: C, 74.1 3; H, 4,75; N, 15.28%.
5b	**MBMQ**	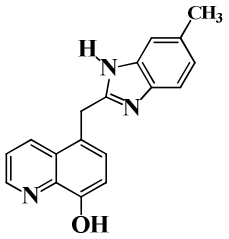	Yield 70 %, M.P. 211 °C, brown of solid. ^{1}H NMR (300 MHz, Me_2SO-d6), δppm = 2.36 (s, 3H, -CH_3); 4.64 (s, 2H, -CH_2-); 6.94-8.83 (m, 8 H_{arm}); 12.27(s, 1H, NH). ^{13}C NMR (300 MHz, Me_2SO-d6), δppm = 22.13 (CH_3); 30.56 (-CH_2-); 112.93-155.5 (CH_{arm} and C_{arm}). Elemental analysis for $C_{18}H_{15}N_3O$: calcd.: C, 74.72; H, 5.23; N, 14.52; Found: C, 74.70; H, 5.26; N, 14.54%.
5c	**CBMQ**	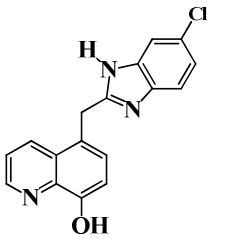	Yield 72 %, M.P. 195 °C, brown of solid. ^{1}H NMR (300 MHz, Me_2SO-d6), δppm = 4,50 (s, 2H,-CH_2-); 6.65-8.81 (m, 8 H_{arm}); 12.20(s, 1H, NH). ^{13}C NMR (300 MHz, Me_2SO-d6), δppm = 34,69(-CH_2-); 110.84-154.01 (CH_{arm} and C_{arm}). Elemental analysis for $C_{17}H_{12}N_3OCl$: calcd.: C, 65.92; H, 3.90; N, 13.57; Found: C, 65.85; H, 3.86; N, 13.59%.
5d	**DCBMQ**	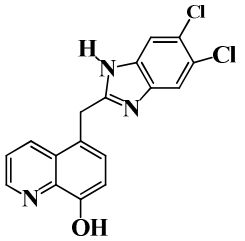	Yield 80 %, M.P. 180 °C, brown of solid. ^{1}H NMR (300 MHz, Me_2SO-d6), δppm = 4.23(s, 2H, -CH_2-); 6.95-8.94 (m, 6H_{arm}). ^{13}C NMR (300 MHz, Me_2SO-d6), δppm = 30,63(-CH_2-);111.90-153.26 (CH_{arm} and C_{arm}). Elemental analysis for $C_{17}H_{11}N_3OCl_2$: calcd.: C, 59.32; H, 3.22; N, 12.21; Found: C, 59.36; H, 3.20; N, 12.23%.

2.2. Materials

The material, on which the review is based, is of the type carbon steel (CS), including its the composition (in wt%) of 0.02 % P, 0.02 % Al, 0.10 % Si, 0.50 % Mn, 0.36 % C, 0.01 % S, 0.2 % Cr and the remainder iron (Fe). 1 cm^2 of working electrode was exposed at aggressive media, this surface area was abraded with different grit SiC paper. This one's was then washed with bi-distilled water and decreased with ethanol.

2.3. Solutions

2 M H_3PO_4 solutions were prepared by dilution of an analytical reagent grade HCl 85% H_3PO_4 with distilled water. The exposure concentrations ranged from 10^{-6} M to 10^{-3} M, these two extremes are used due to the solubility and the minimum protection.

2.4. Electrochemical measurements

The 1 cm^2 of CS surface is employed as working electrode. A platinum wire was operated as a counter electrode; a saturated calomel electrode was employed as a reference electrode booster by Luggin capillary.

At the beginning, the exposed area of steel was immersed in electrolyte for half hour till you get steady state open circuit potential (E_{ocp}), and that is when the electrochemical measurements were carried out. The electrochemical assays were carried out under aerated solution and thermostatic conditions. The EIS assays were realized in the frequency interval of 10^5 Hz to 0.1 Hz at E_{ocp} with amplitude of 10 mV. The ZView software was used to precede impedance spectra. The protection efficiency $\eta_Z(\%)$ of EIS is defined by the formula below:

$$\eta_Z(\%) = \frac{R_{P(i)} - R_p}{R_{P(i)}} \times 100 \quad (1)$$

where R_p and $R_{p(i)}$ are the ac polarization resistance of CS electrode without and with synthesized molecules, respectively.

The Tafel curves were registered from cathodic to the anodic direction, with a scan rate of 0.5 mV s^{-1} and analyzed by means of Voltamaster 4 software. The inhibition efficiency for three kinds of 8-hydroxyquinoline derivatives was also elaborated according to the Tafel curves:

$$\eta_{\text{Tafel}}(\%) = \frac{i_{\text{corr}} - i_{\text{corr(i)}}}{i_{\text{corr}}} \times 100 \quad (2)$$

where i_{corr} and $i_{\text{corr(i)}}$ are the corrosion current densities in the absence and the presence of 8-hydroxyquinoline derivatives, respectively.

2.5. Surface analyses

Scanning Electron Microscopy (JEOL 5300) was employed in assessing the surface quality of CS substrate without and with four kinds of 8-hydroxyquionline and after been immersed in 2 M H_3PO_4.

X-ray photoelectron spectroscopy (XPS) spectra were registered using XPS KRATOS, AXIS Ultra^{DLD} spectrometer Thermo Scientific K-Alpha XPS system. The XPS test and treatment were made according to the same procedures previously described [40,41].

2.6. Density functional theory calculations

Molecules of BIMQ, CBMQ, DCBMQ and MBMQ were modelled with GaussView 5.0 and subjected to geometry optimizations without symmetry constraints using the B3LYP/6-31+(d,p) model [42-44]. Since the experimental studies were carried out in aqueous phosphoric acid medium, all geometry optimizations were conducted in phosphoric acid medium, which was simulated by setting the solvent parameters of aqueous H_3PO_4 as 62.4 and 2.054 for static and optical dielectric constants respectively. The static dielectric constant was extracted from literature [45], while the optical dielectric constant was approximated as the square of refractive index (n20/D = 1.433) of phosphoric acid as previously proposed in the literature [46,47]. All the calculations were carried out using Gaussian 09 [48] and the polarizable continuum model (PCM) using the integral equation formalism variant (IEFPCM) implemented in Gaussian 09 was used to treat the solvent. Relevant quantum chemical

parameters were derived from the frontier molecular orbitals (FMOs) energies, that is, highest occupied molecular orbital energy (E_{HOMO}) and lowest unoccupied molecular orbital energy (E_{LUMO}) of the optimized structures based on the following relations [49]:

(Energy gap, ΔE) : $$\Delta E = E_{LUMO} - E_{HOMO} \quad (3)$$

(Global hardness, η) : $$\eta = -\frac{1}{2}(E_{LUMO} - E_{HOMO}) \quad (4)$$

(Global electronegativity, χ) $$\chi = -\frac{1}{2}(E_{LUMO} + E_{HOMO}) \quad (5)$$

(Fraction of electron transferred) $$\Delta N = \frac{\phi_{Fe} - \chi_{inh}}{2(\eta_{Fe} + \eta_{inh})} \quad (6)$$

where $\Phi_{Fe(110)}$ and η_{Fe} are the work function and hardness of Fe respectively, while χ_{inh} and η_{inh} are the electronegativity and hardness of the inhibitor molecule respectively. A value of 4.82 eV for $\Phi_{Fe(110)}$ (previously reported for body center cubic (bcc) crystal structure of Fe(110)) [50,51] and a value of 0 eV/mol [52] for η_{Fe} were used in Equation 6 based on previous studies [49-52].

2.7. Monte Carlo simulation

Adsorption of BIMQ, CBMQ, DCBMQ and MBMQ molecules on mild steel surface in phosphoric acid medium was using the adsorption locator module available in Materials Studio 2106. Mild steel is essentially iron, and thus, steel surface was represented by (1 1 0) cleaved plane of Fe, which has been adjudged the most reasonable crystal plane for the metal. The optimized structures of the inhibitor molecules obtained from the DFT study were used in the Monte Carlo simulations. To ensure that the simulation was as close as possible to the experimental study, the adsorption of each inhibitor molecule on Fe(110) was simulated in the presence of phosphoric acid solution, which was represented by H_3O^+ and PO_4^{3-} ions.

Iron crystal was first cleaved into (1 1 0) plane, optimized and expanded into a 10 × 10

supercell having 6 layers of crystals in a 10 Å vacuum slab. H_3O^+ and PO_4^{3-} were optimized using the Universal force field in Forcite module. Adsorption of 60 molecules of H_3O^+ and 60 molecules of PO_4^{3-} (since H^+ and PO_4^{3-} are in ratio 3:1 in one mole of the acid) on Fe(110) was first simulated in a simulated annealing using the COMPASSII force field. The simulation was carried out for 5 cycles at 50000 steps per cycles. Thereafter the inhibitor molecule was adsorbed using the same computational details. The adsorption energy was calculated according to equation (7):

$$E_{ads} = E_{complex2} - E_{complex1} \quad (7)$$

where $E_{complex2}$ is the total energy of the Fe (110)/inhibitor/20 PO_4^{3-}/60 H_3O^+ complex and $E_{complex1}$ is the total energy of the Fe (110)/20 PO_4^{3-}/60 H_3O^+ complex.

3. Results and discussion

3.1. Corrosion inhibition studies

3.1.1. Polarization measurements

The cathodic and anodic Tafel curves for working electrode dipped in 2 M H_3PO_4 including and excluding different concentrations of BIMQ, MBMQ, CBMQ and DCBMQ are illustrated in Fig. 1, it is clear that this is a significant decrease in the two cathodic and cathodic densities after addition of these four 8-hydroxyquinoline derivatives, which implies that the synthesized 8-hydroxyquinoline derivatives prevents both the iron dissolution and the cathodic hydrogen evolution. On the other hand, the prevention of the cathodic reaction is important in comparison that anodic reaction to cause a shift of corrosion potential towards the negative direction, The negative displacement of E_{corr} after adding 8-hydroxyquinoline derivatives is $\leq$ 85 mV, indicating that these 8-hydroxyquinoline derivatives are acting like mixed-type inhibitors with predominant cathodic effectiveness [53]. Various extrapolated parameters from Tafel curves are included in Table 2.

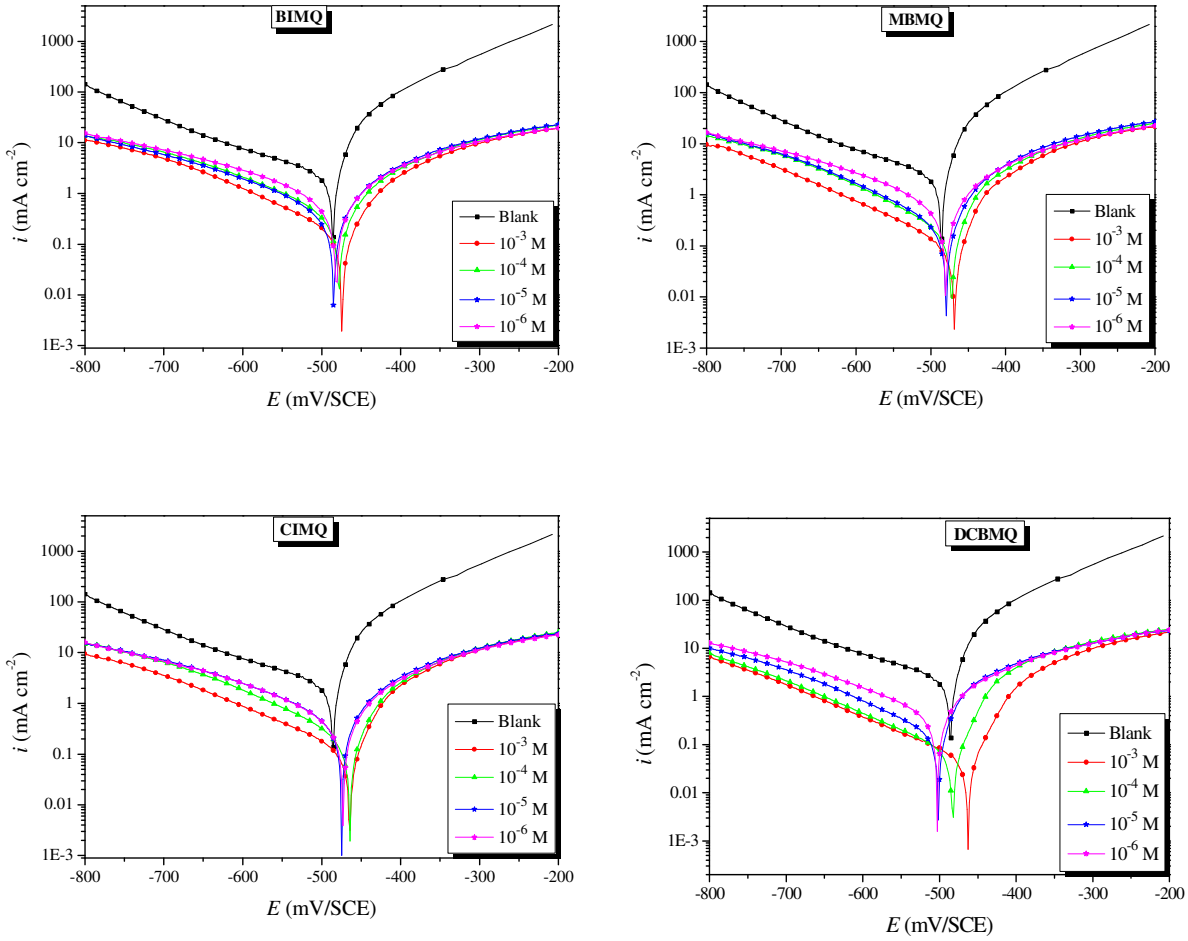

Fig. 1. Tafel plots for CS in 2 M H_3PO_4 prior to and after adding of various concentrations of BIMQ, MBMQ, CBMQ and DCBMQ.

Results in Table 2 indicate a significant reduction of i_{corr} upon addition of four kind 8-hydroxyquinoline compared with that of the blank electrolyte. This large reduction is approximately forty-two times in case of DCBMQ at 10^{-3} M, the increase in concentration causing a protective film covers the CS surface producing a decrease in corrosion current density. The values of β_c are changed following the addition of four kinds of 8-hydroxyquinoline which suggests that this is an alteration of cathodic reaction [54,55].

The effectiveness ranking of four studied organic compounds at all concentrations is as per the following: DCBMQ > CBMQ > MBMQ > BIMQ, this order is assigned to the differences in the structures among the four 8-hydroxyquinoline derivatives. Additionally, it's

clear that all the inhibitors tested have a similar structure with the exception of alkyl substituent carrying by the phenyl of benzimidazole. An extensively, it is found that the substitution of H in aromatic ring of benzimidazole moiety of compound BIPQ by methyl in MBMQ, chlorine in CBMQ and two chlorine atoms in DCBMQ change the protection efficiency. The presence of chlorine atoms which are donor by mesomeric effect (+M) in aromatic ring of CBMQ and DCBMQ increases the delocalization of electron density in the molecule, which makes the molecule more stable. This adsorption can be stabilized by participation of π-electrons of aromatic ring and free electron pair in the heteroatom.

Table2

Various extrapolated parameters of CS prior to and after adding different concentrations of 8-hydroxyquinoline derivatives in 2 M H_3PO_4 electrolyte.

Inhibitor	C_{inh} (M)	$-E_{corr}$ (mV/SCE)	i_{corr} (μA/cm^2)	$-\beta_c$ (mV/dec)	η_{Tafel} (%)
Blank	—	419	2132.0	219.6	—
BIMQ	10^{-3}	477	156.2	137.3	93.0
	10^{-4}	481	382.0	162.5	82.1
	10^{-5}	490	420.0	168.6	80.3
	10^{-6}	482	615.3	170.7	71.1
MBMQ	10^{-3}	472	120.0	136.9	94.4
	10^{-4}	476	184.5	138.2	91.3
	10^{-5}	482	232.6	138.5	89.1
	10^{-6}	483	521.4	161.8	75.5
CBMQ	10^{-3}	469	112.0	146.8	94.7
	10^{-4}	469	199.5	147.0	90.6
	10^{-5}	479	382.0	156.8	82.1
	10^{-6}	478	429.5	160.0	79.8
DCBMQ	10^{-3}	467	51.0	127.2	97.6
	10^{-4}	486	71.2	146.4	96.7
	10^{-5}	505	161.7	158.7	92.4
	10^{-6}	507	397.9	166.2	81.3

3.1.2. Electrochemical impedance spectroscopy studies (EIS)

3.1.2.1. Effect of inhibitor concentration

Nyquist diagrams of CS in H_3PO_4 electrolyte in the absence and presence diverse concentrations of 8-hydroxyquinoline derivatives are provided in Fig. 2. All diagrams showed

two semicircles, one at the high frequency (HF) and the other at the low frequency (LF) region. The obtained semicircle at high frequency is allocated to the charge-transfer and double layer capacitance at the CS/electrolyte interface for the corrosion mechanism [56-58]. While that the inductive loop at low frequency may be assigned to the relaxation process achieved through adsorption of the chemical species like products of the corrosion reaction (exp. ferric phosphate), an oxidizable or reducible intermediate [59] or neutral or/and ionic forms of 8-hydroxyquinoline derivatives [60] on the CS surface.

The existing HF loops are slightly depressed in real axis and non-perfect semi-circles demonstrate the roughness and/or inhomogeneity of the CS surface [61]. As consequence, CPE was inserted in the equivalent circuit to substitute the double layer capacitance in order to obtain a good fit and which is defined through next formula [62-64]:

$$Z_{CPE} = A^{-1}(i\omega)^{-n} \quad (8)$$

where A and n presents the constant and exponent of CPE, respectively. i is the imaginary number and ω (rad s^{-1}) is the radial frequency.

The selected equivalent circuit (Fig. 3) to fit the experimental EIS data consists of electrolyte resistance (R_s) in series with CPE in parallel with charge transfer resistance (R_{ct}) in series with an inductive resistance R_L in parallel with an inductance (L). However, the (R_{ct} + R_L) present the polarization resistance (R_p). These cited parameters are summarized in Table 3.

These cited parameters are summarized in Table 3. From this table, there are also the values of C_{dl} which are derived from the CPE constant by virtue of the next formula [65, 66]:

$$C_{dl} = (AR_p^{1-n})^{1/n} \quad (9)$$

The collected value of C_{dl} and R_p are exploited to establish the relaxation time constant (τ_d) in line with to the following equation [67,68]:

$$\tau = C_{dl} R_p \quad (10)$$

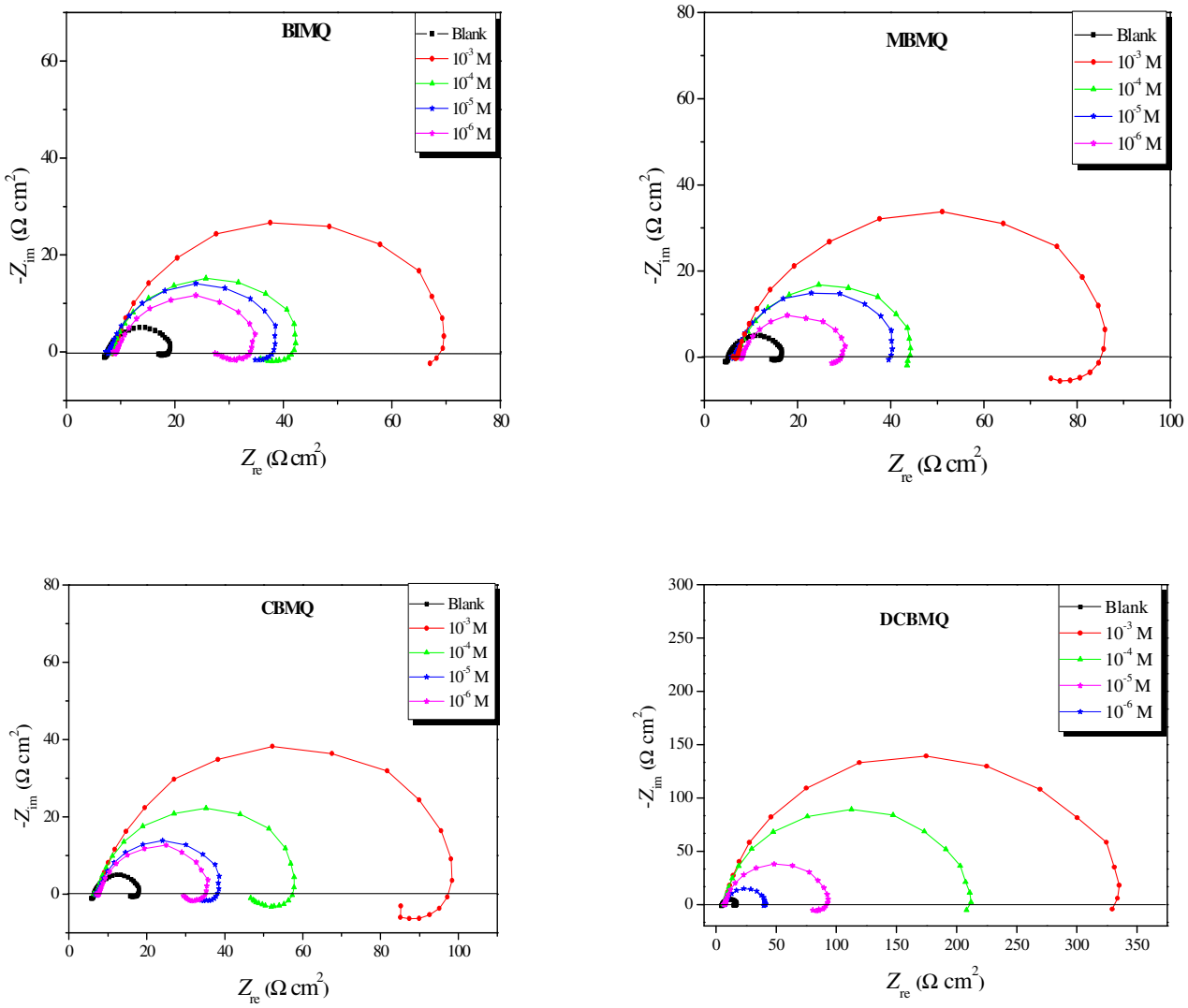

Fig. 2. Nyquist plots of the CS substrate in 2 M H_3PO_4 with BIMQ, MBMQ, CBMQ and DCBMQ at different concentrations at 303 K.

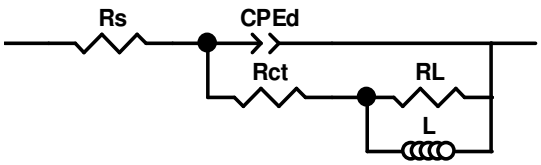

Fig. 3. Equivalent circuit employed for adjusting the impedance data.

The fits of our data using the present circuit are very satisfactory; a typical example of Nyquist and Bode diagrams fitted is presented in Fig. 4. Based on the Table 3, the assembled values of A and C_{dl} are inversely proportionate to with inhibitor concentration, while R_p, R_L, n, L, τ_d, $\eta_Z(\%)$ are diverse in the same manner with the concentration of four 8-hydroxyquinoline derivatives. The increasing R_p achieved 330.42 (Ω cm^2) in case of DCBMQ involves the formation of the protective film [69]. Furthermore, the rise of the values of n after addition of synthesized compounds when compared with 2 M H_3PO_4 could be explained away by certain decrease of the working electrode surface heterogeneity because of the occupation of most active adsorption sites by 8-hydroxyquinoline derivatives. The C_{dl} values in presence of studied molecules are lower than that of blank electrolyte could be through the reduction in local dielectric constant as a result of a substitution of H_2O by inhibitors molecules at CS surface [70]. Moreover, the augmentation of the relaxation time constant (τ_d) with 8-hydroxyquinoline derivatives concentration suggests that the time of adsorption process gets slower. The corresponding L values for CS are observed to improve with addition of 8-hydroxyquinoline derivatives in 2 M H_3PO_4 electrolyte that may be due to an increase of oxidizable or reducible intermediate of 8-hydroxyquinoline derivatives in the electrolyte. Considering the EIS results, it's obvious that the η_Z (%) with increases with concentration for four kinds of 8-hydroxyquinoline derivatives, this might be because the protonation of the heteroatoms (the aromatic amino group) presents in inhibitory molecules reducing the concentration of the hydrogen proton of electrolyte. From EIS findings, the sequence of inhibitor performance is DCBMQ > CBMQ > MBMQ > BIMQ. This is consistent with the

obtained data by potentiodynamic polarization experiments. Obviously, the maximum effeteness corresponding at 10^{-3}M for the four inhibitors and therefore, this optimum concentration was chosen to investigate the influence of temperature.

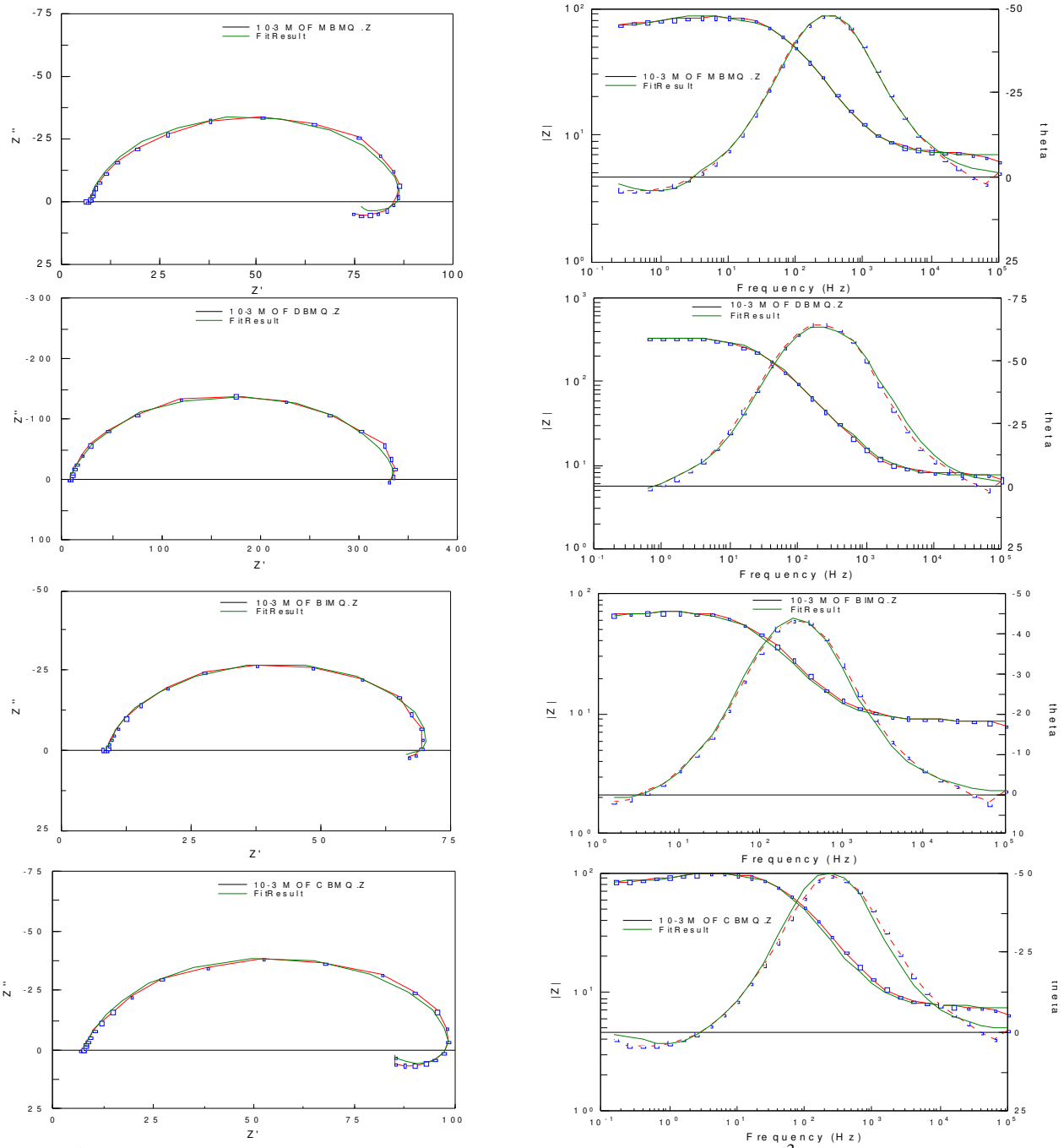

Fig. 4. EIS Nyquist and Bode diagrams for CS/2 M H_3PO_4 + 1×10^{-3} M BIMQ, MBMQ, CBMQ and DCBMQ interface: (red line) experimental data and (green Line) calculated.

Table 3
EIS results for CS in 2 M H_3PO_4 in the absence and presence of different concentrations of the synthesized 8-hydroxyquinoline derivatives at 303 K.

Inhibitor	C_{inh} (M)	R_s (Ω cm^2)	R_{ct} (Ω cm^2)	R_L (Ω cm^2)	R_p (Ω cm^2)	10^4 A (Ω^{-1} S^n cm^2)	n	L (H cm^{-2})	C_{dl} (μF cm^{-2})	τ_d (ms)	η_Z (%)	θ
2 M H_3PO_4	—	5.21± 0.02	9.71 ± 0.06	2.01 ± 0.08	11.72	2.43 ± 0.09	0.880± 0.005	0.19± 0.02	109.2	1.22	—	—
BIMQ	10^{-6}	7.27 ± 0.07	19.58 ± 0.27	5.83 ± 0.37	25.41	0.75 ± 0.07	0.898± 0.010	0.14± 0.17	36.8	0.94	53.8	0.54
	10^{-5}	7.85 ± 0.06	27.30 ± 0.36	4.88 ± 0.53	32.20	0.73 ± 0.05	0.892± 0.010	0.33± 0.08	32.5	1.05	63.6	0.64
	10^{-4}	8.40 ± 0.06	28.41 ± 0.38	6.40 ± 0.48	34.81	0.62 ± 0.04	0.901± 0.009	0.38± 0.13	30.0	1.10	66.3	0.66
	10^{-3}	8.67 ± 0.06	56.53 ± 0.42	7.65 ± 0.52	64.18	0.60 ± 0.03	0.905± 0.007	0.43± 0.18	28.1	1.80	81.7	0.82
MBMQ	10^{-6}	6.39 ± 0.06	19.44 ± 0.35	3.61 ± 0.41	23.05	0.83 ± 0.08	0.890± 0.020	0.20± 0.03	35.7	0.82	49.1	0.49
	10^{-5}	6.43 ± 0.05	32.97 ± 0.53	3.99 ± 0.63	36.96	0.78 ± 0.07	0.898± 0.010	0.41± 0.03	35.1	1.29	68.3	0.68
	10^{-4}	6.90 ± 0.06	34.34 ± 0.59	5.20 ± 0.68	39.54	0.68 ± 0.05	0.899± 0.009	0.52± 0.10	30.3	1.20	70.3	0.70
	10^{-3}	6.92 ± 0.06	67.05 ± 0.62	15.77 ± 0.73	82.82	0.62 ± 0.03	0.908± 0.006	2.31± 0.40	26.0	2.15	86.0	0.86
CBMQ	10^{-6}	6.63 ± 0.06	22.71 ± 0.29	5.67 ± 0.39	28.38	0.66 ± 0.05	0.897± 0.001	0.77± 0.12	29.4	0.83	60.5	0.60
	10^{-5}	6.96 ± 0.06	26.79 ± 0.37	5.49 ± 0.46	32.28	0.65 ± 0.05	0.892± 0.009	1.52± 0.10	28.6	0.92	63.7	0.64
	10^{-4}	7.04 ± 0.06	41.25 ± 0.43	10.80 ± 0.64	52.05	0.59 ± 0.03	0.896± 0.008	2.16± 0.30	28.2	1.46	77.4	0.77
	10^{-3}	7.22 ± 0.05	77.33 ± 0.83	18.56 ± 0.89	95.89	0.56 ± 0.03	0.906± 0.006	2.72± 0.41	21.5	2.06	88.3	0.88
DCBMQ	10^{-6}	7.22 ± 0.05	32.02 ± 0.61	2.22 ± 0.61	34.24	0.68 ± 0.04	0.894± 0.008	0.71± 0.47	33.1	1.13	65.7	0.66
	10^{-5}	7.24 ± 0.06	73.68 ± 0.63	14.02 ± 1.34	87.20	0.57± 0.02	0.901± 0.006	4.54± 0.60	31.4	2.73	86.5	0.86
	10^{-4}	7.46 ± 0.06	176.00 ± 0.59	32.61± 0.30	208.61	0.33 ± 0.01	0.920± 0.005	11.75± 0.65	21.4	4.46	94.4	0.94
	10^{-3}	7.60 ± 0.06	284.60 ± 0.67	45.82 ± 0.91	330.42	0.31± 0.09	0.950± 0.004	30.05±0.91	18.7	6.17	96.4	0.96

3.1.2.2. Effect of electrolyte temperature

Figs. 5 and 6 show Nyquist graphics for CS in 2 M H_3PO_4 pre- and post- addition of 10^{-3} M of DCBMQ, CBMQ, MBMQ and BIMQ at 303 K-333 K range. A really good fit for all collected EIS data was obtained with the model proposed early.

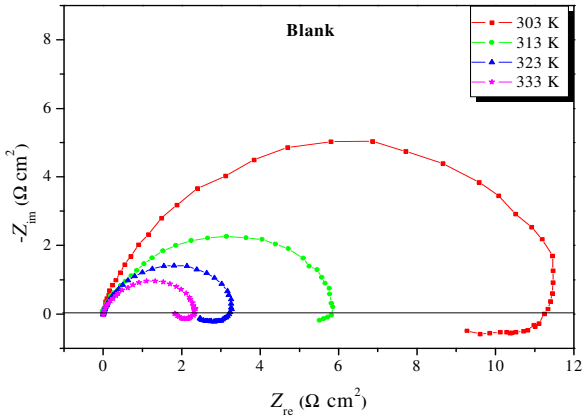

Fig. 5. Nyquist diagrams for CS substrate in 2 M H_3PO_4 at different temperatures.

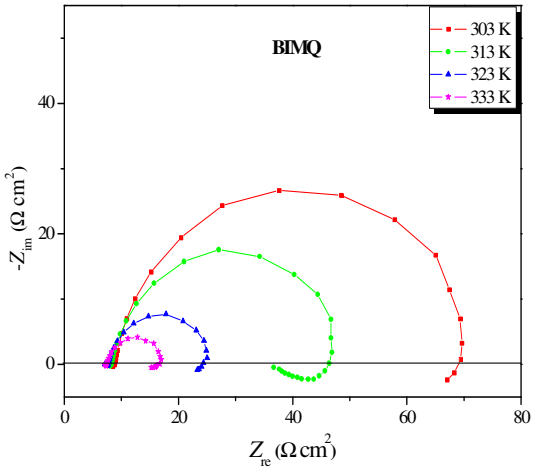

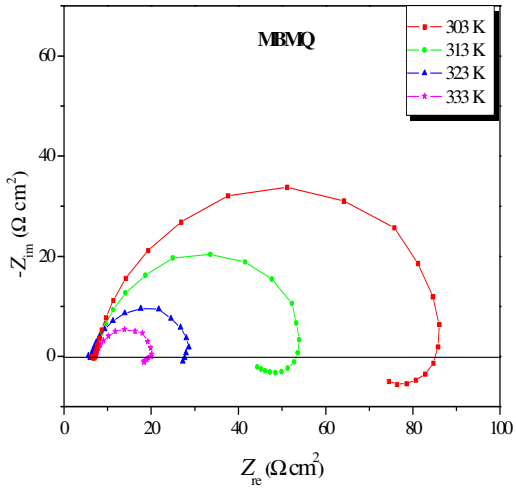

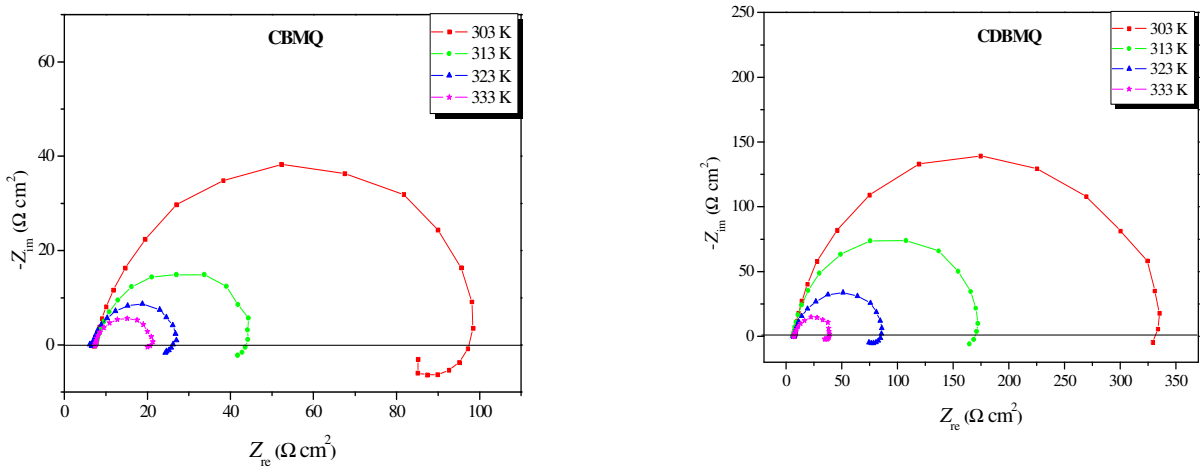

Fig. 6. Nyquist plots for CS in 2 M H_3PO_4 medium containing 10^{-3} M of various synthesized 8-hydroxyquinoline derivatives at different temperatures.

The spectrum impedance in both prior to and subsequent to the addition of 8-hydroxyquinoline derivatives exhibit also two single, the first capacitive loop at a high-medium frequency and the second inductive loop at low frequency. The high-medium frequency capacitive semi-circle is connected to the charge transfer process. The low-frequency inductive semi-circle may be a result of the relaxation process brought about by the ions of the inhibitors. The size of the capacitive loop declines with increasing temperature in both inhibited and uninhibited electrolytes. The extracted corrosion parameters are collected in Table 4. The inspection of the latter demonstrated that, the temperature rise prompts a diminishing of R_p values, initially explained by the increase of the rate of metal dissolution, secondly by the displacement of the adsorption/desorption equilibrium verse the inhibitor desorption and consequently an abatement of surface coverage degree. Besides, the n value declined with temperature increasing, which construed as a proves for the surface inhomogeneity increase. Furthermore, the η_Z (%) for four synthesized 8-hydroxyauinoline derivatives reveals a smaller fall at 303-333K range (decreased to 90.8% for DCBMQ, 82.2% for both CBMQ/MBMQ and 77.2% for BIMQ at optimum concentration in 333 K), indicating

that the four synthesized 8-hydroxyauinoline derivatives keep their stability and their the inhibitive performance under these conditions.

Values of R_p were utilized to estimated values of the corrosion current density (i_{corr}) at divers' temperatures including and excluding of inhibitors using the next equation [49]:

$$i_{corr} = RT\,(zFR_p)^{-1} \quad (11)$$

where R is an ideal gas constant (R = 8.314 J mol^{-1} K^{-1}), F is the Faraday constant (F = 96 485 C) and z is the valence of iron metal (z = 2).

Table 4

The corresponding EIS parameters at 303-333 K range of CS in 2 M H_3PO_4 including and excluding 10^{-3} M of four 8-hydroxyquinoline derivatives.

Inhibitor	Temp. (K)	R_s (Ω cm^2)	R_{ct} (Ω cm^2)	R_L (Ω cm^2)	R_p (Ω cm^2)	$10^4 A$ (Ω^{-1} S^n cm^2)	n	L (H cm^{-2})	C_{dl} (μF cm^{-2})	τ_d (ms)	η_Z (%)
	303	5.21 ± 0.02	9.710 ± 0.060	2.010 ± 0.080	11.72	2.430 ± 0.090	0.880 ± 0.005	0.19 ± 0.02	109.2	1.22	—
2 M H_3PO_4	313	4.28 ± 0.01	5.590 ± 0.044	0.560 ± 0.049	6.15	3.689 ± 0.360	0.879 ± 0.066	0.037 ± 0.036	159.6	0.98	—
	323	2.79 ± 0.02	2.629 ± 0.054	0.723 ± 0.069	3.35	4.786 ± 0.730	0.878 ± 0.020	0.053 ± 0.011	195.7	0.66	—
	333	3.79 ± 0.01	1.855 ± 0.019	0.416 ± 0.019	2.27	6.068 ± 0.270	0.875 ± 0.011	0.037 ± 0.004	236.0	0.54	—
	303	8.67 ± 0.06	56.530 ± 0.420	7.650 ± 0.520	64.18	0.600 ± 0.030	0.905± 0.007	0.43± 0.18	28.1	1.80	81.7
BIMQ	313	8.238 ± 0.070	29.420 ± 0.342	3.300 ± 0.510	32.72	0.748 ± 0.040	0.878 ± 0.009	0.47 ± 0.150	32.43	1.06	81.2
	323	7.617 ± 0.050	14.360 ± 0.317	2.250 ± 0.380	16.61	0.908 ± 0.090	0.873 ± 0.013	0.034 ± 0.01	35.28	0.58	79.8
	333	7.397 ± 0.050	08.100 ± 0.168	1.844 ± 0.200	9.94	1.027 ± 0.150	0.868 ± 0.017	0.020 ± 0.04	36.03	0.36	77.2
	303	6.92 ± 0.06	67.050 ± 0.620	15.770 ± 0.730	82.82	0.620 ± 0.030	0.908± 0.006	2.31± 0.40	26.0	2.15	86.0
MBMQ	313	7.010 ± 0.062	36.430 ± 0.520	06.710 ± 0.710	43.14	0.736 ± 0.050	0.850 ± 0.008	0.93 ± 0.13	26.67	1.19	85.7
	323	6.136 ± 0.060	18.580 ± 0.636	3.860 ± 0.681	22.45	0.910 ± 0.010	0.846 ± 0.014	0.04 ± 0.016	29.47	0.66	85.0
	333	7.169 ± 0.060	09.960 ± 0.247	2.839 ± 0.310	12.80	1.000 ± 0.020	0.845 ± 0.016	0.03 ± 0.006	29.49	0.37	82.2
	303	7.22 ± 0.05	77.330 ± 0.830	18.560 ± 0.890	95.89	0.560 ± 0.030	0.906± 0.006	2.72± 0.41	21.5	2.06	88.3
CBMQ	313	7.576 ± 0.060	32.870 ± 0.870	7.241 ± 0.840	40.11	0.640 ± 0.050	0.885 ± 0.009	0.193 ± 0.06	29.47	1.18	84.7
	323	6.703 ± 0.060	16.000 ± 0.420	4.100 ± 0.456	20.01	0.749 ± 0.080	0.883 ± 0.013	0.077 ± 0.02	31.66	0.64	83.3
	333	7.472 ± 0.050	10.460 ± 0.620	2.328 ± 0.520	12.78	0.935 ± 0.090	0.879 ± 0.014	0.023 ± 0.01	37.04	0.47	82.2
	303	7.60 ± 0.06	284.60 ± 0.67	45.82 ± 0.91	330.42	0.310 ± 0.090	0.950± 0.004	30.05±0.91	18.7	6.17	96.4
DCBMQ	313	6.433 ± 0.060	151.30 ± 0.59	14.23 ± 0.99	165.53	0.396 ± 0.010	0.900 ± 0.005	1.801 ± 0.93	22.65	3.74	96.2
	323	6.770 ± 0.060	73.12 ± 0.58	10.15 ± 0.94	83.27	0.683 ± 0.040	0.858 ± 0.007	0.587 ± 0.22	29.03	2.41	95.9
	333	7.080 ± 0.068	27.54 ± 0.53	06.61 ± 0.64	34.15	0.853 ± 0.070	0.855 ± 0.011	0.445 ± 0.09	30.92	1.05	90.8

The i_{corr} values are used to estimate the apparent activation energy E_a according to the according to the formula below [71].

$$i_{corr} = k \exp\left(\frac{-E_a}{RT}\right) \quad (12)$$

where k is the Arrhenius pre-exponential factor. Additionally, the variation of apparent enthalpy (ΔH_a) and apparent entropy (ΔS_a) for the establishment of the activation complex in the transition state possibly determined through the above transition-state equation:

$$i_{corr} = \frac{RT}{Nh} \exp\left(\frac{\Delta S_a}{R}\right) \exp\left(-\frac{\Delta H_a}{RT}\right) \quad (13)$$

where N and h are the Avogadro's and the Plank's constants, respectively.

The variation of i_{corr} as a function $1/T$ in both before and since the synthesized compounds match a straight line whose slope equal $-E_a/R$. A graphic of Ln (i_{corr}/T) versus $1/T$ match a straight line whose slope of ($-\Delta H_a/R$) and intercept of (Ln R/Nh + $\Delta S_a/R$). Both graphics are illustrated in Figs. 7 and 6. The estimated values of E_a, ΔH_a and ΔS_a are summariZed in Table 5. The estimated values of E_a for CS in the presence of four kinds of 8-hydroxyquinoline derivatives are superior to that of 2 M H_3PO_4 electrolyte. Szauer et al. have clarified that the growing in E_a may be related to a reduced in the adsorption process with increasing temperature [71]. Additionally, the increase value of the E_a may be explained by the proceeding of specific interaction between inhibitor/electrode surface and with electrostatic adsorption, correspondingly. The organic molecules studied have weak basic properties, which promote their protonation in an acidic medium [72]. Mostly attacking the nitrogen atom (N) in the rings imidazole and pyridine moieties, subsequently, they become ionized, that are in equilibrium with the corresponding molecular form (Scheme 2):

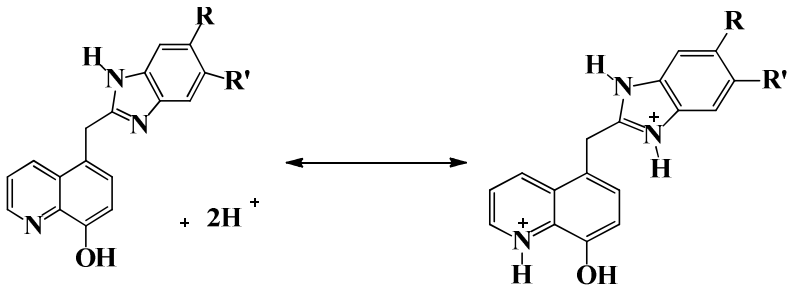

Scheme 2. Protonation of DCMBQ molecule in 2 M H_3PO_4 medium.

Therefore, the solution will contain both the molecular and the cationic forms of the compounds, Moreover, there are specifically adsorbed phosphate ions (they come from the supporting electrolyte, which are usually characterized by low adsorbability). Thus, he appears reasonable to suggest an electrostatic type of adsorption.

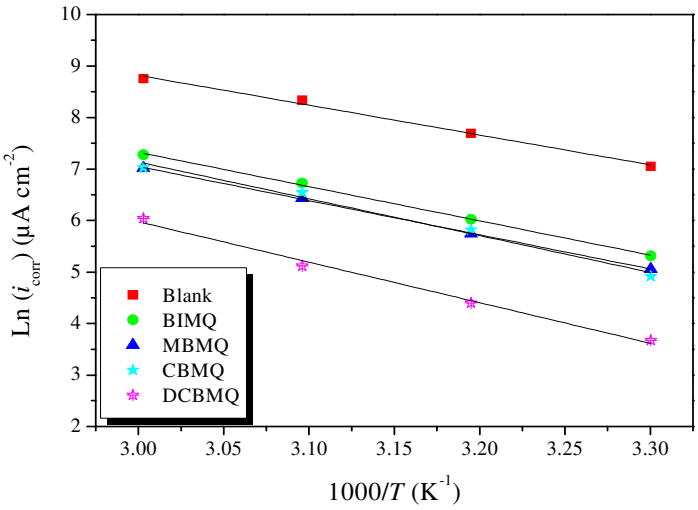

Fig. 7. Ln (i_{corr}) versus 1/T in 2 M H_3PO_4 without and with of optimum concentration of 8-hydroxyquinoline derivatives.

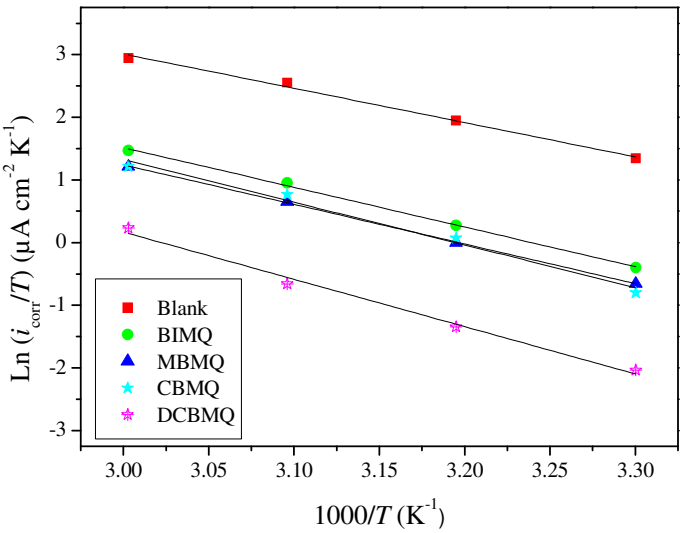

Fig. 8. Ln(i_{corr}/T) versus 1/T in 2 M H_3PO_4 without and with of optimum concentration of synthesized 8-ydroxyquinoline derivatives.

Table 5

Activation parameters for CS substrate in 2 M H_3PO_4 in the absence and presence of optimum concentrations of 8-hydroxyquinoline derivatives.

Medium	R^2	E_a (kJ mol^{-1})	ΔH_a (kJ mol^{-1})	ΔS_a (J mol^{-1} K^{-1})
Blank	0.993	48.14	45.50	-36.02
BIMQ	0.998	55.32	52.68	-23.90
MBMQ	0.999	55.13	52.49	-29.75
CBMQ	0.984	59.39	56.75	-16.26
DCBMQ	0.988	65.39	62.74	-07.92

Based on the absolute value of ΔH_a it is possible to differentiate between the chemisorption and the physisorption process. For a physisorption adsorption the enthalpy is equal to or lower than 40 100 kJ mol^{-1} while, a chemisorption it is equal to or higher than 100 kJ mol^{-1} [72,73]. The obtained values of ΔH_a for all synthesized compounds are superior 40 but lower than 100 kJ mol^{-1} suggest that the adsorption model is combination of physisorption and chemisorption [74]. The ΔS_a values of DCBMQ, CBMQ, MBMQ, BIMQ, and 1M HCl electrolyte are negatives, which reveal that the activated complex in the rate-determining step stands for an association rather than dissociation. The values of the activation energy are superior for

inhibited solutions than for uninhibited solution. This could be the result of the adsorption of four kinds of benzimidazole derivatives on the CS surface, which could be considered a replacement process of water molecules during adsorption of benzimidazole derivatives on the CS surface. This observation is in agreement with the findings of other workers [75,20].

3.2. Adsorption phenomenon

The scanning electron microscopy (SEM) was realized so as to investigate the impact of different 8-hydroxyquinoline derivatives upon the steel surface morphology. The SEM observations (Figs. 9a-f) of the CS substrate surfaces were taken at same amplification (× 1100) so as to see the progressions that occurred over corrosion process in the presence and non-attendance of the studied inhibitors in 2 M H_3PO_4 electrolyte. The immerged metal surface in H_3PO_4 solution without inhibitor was emphatically harmed (Fig. 9b) compared to the slick and uniform metal surface with just little scratches by abrasive grains before the immersion (Fig. 9a). After added 10^{-3} M of investigated compounds, the damage level of metal surface is astoundingly decreased, which justify the effect inhibitive of studied molecules. Besides, the metal surface in presence of DCBMQ is very smooth and less damaged than other inhibitors.

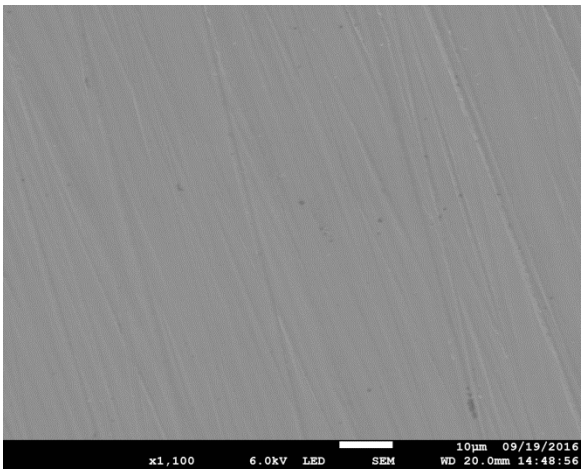

a

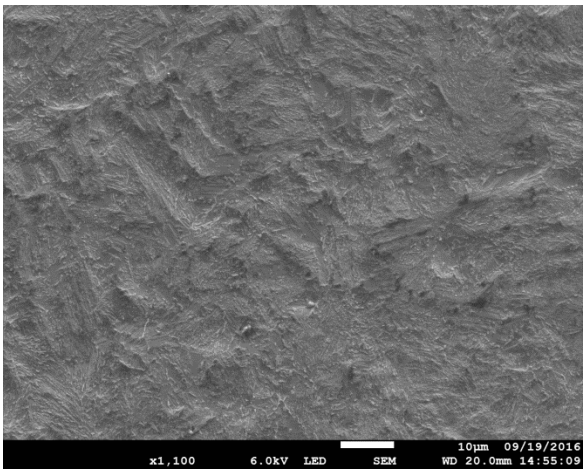

b

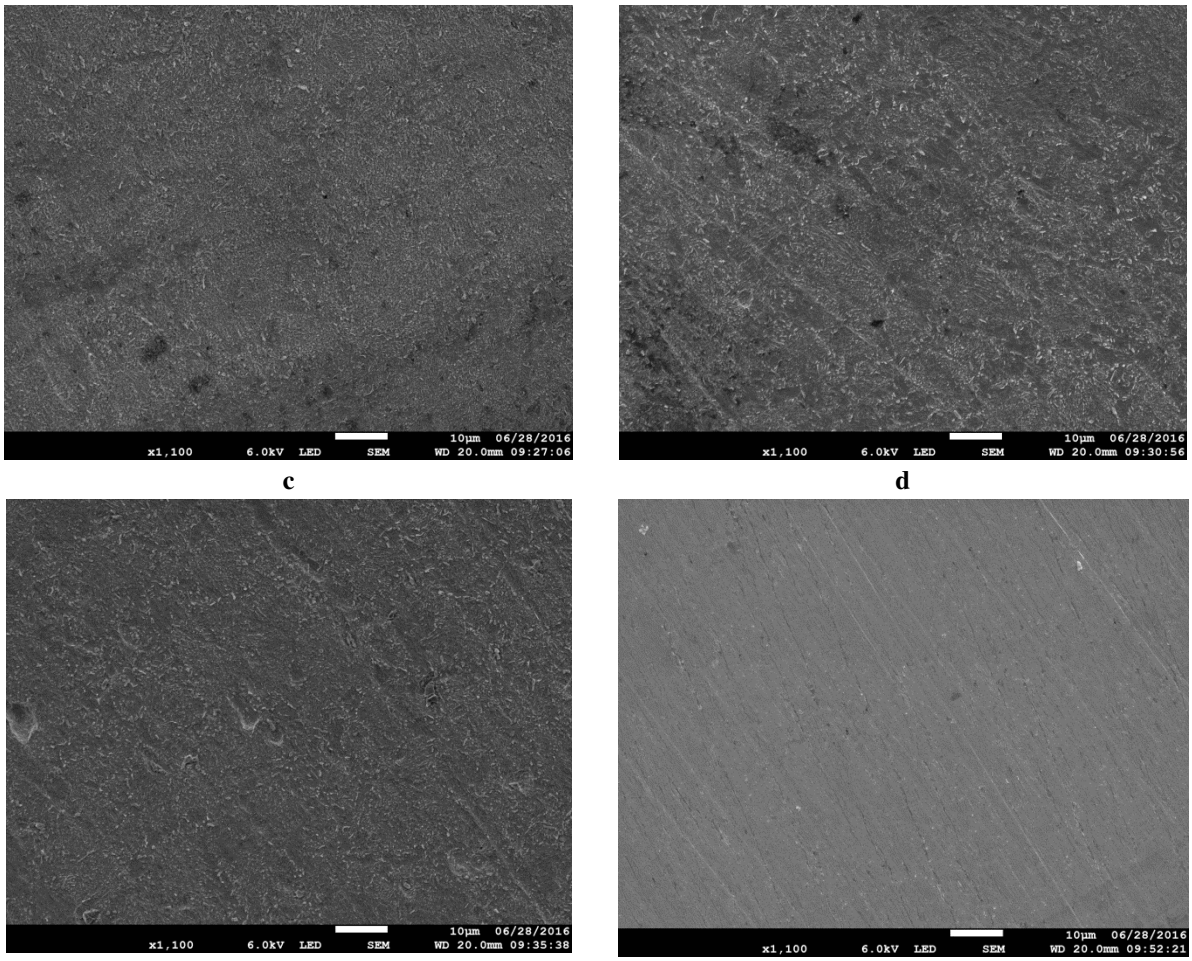

Fig. 9. SEM micrographs of CS surface: a) just after being polished, b) after 6 h immersion in 2 M H_3PO_4 and after 6 h of immersion in 2 M H_3PO_4 containing 10^{-3} M of c) BIMQ, d) MBMQ, e) CBMQ and f) DCBMQ.

The new synthesized 8-hydroxyquinoline derivatives containing benzimidazole moiety restrain corrosion of the CS by adsorbing onto the metal surface in a corrosive electrolyte. To clear up this adsorption process, various models of adsorption isotherms can be utilized, a better fit of EIS data was obtained through the Langmuir isotherm, which is defined by Eq. 14 [76]:

$$\frac{C_{inh}}{\theta} = \frac{1}{K_{ads}} + C_{inh} \quad (14)$$

where K_{ads} named the equilibrium constant for the adsorption process, θ is the surface coverage which is represented by next formula (15):

$$\theta = \frac{\eta_Z(\%)}{100} \quad (15)$$

The K_{ads} values are connected with free energy of adsorption (ΔG^{o}_{ads}) according to the following equation [76]:

$$K_{ads} = \frac{1}{55.55}\exp\left(\frac{-\Delta G^{o}_{ads}}{RT}\right) \quad (16)$$

where R is defined as constant molar gas and 55.55 is the concentration of water in solution in mol L^{-1}.

The analysis of Fig. 10 shows that for all the compounds the variation of the ratio C_{inh}/θ as a function of C_{inh} is linear. This indicates that the adsorption of 8-hydroxyquinoline derivatives on the CS surface in phosphoric medium obeys the Langmuir adsorption isotherm. Therefore, the inhibition of corrosion is due to the formation of a single layer on the CS surface [77], limiting the access of the electrolyte. The regression coefficients (R^2) are all close to 1 ($R^2 > 0.999$), confirming the validity of the chosen model.

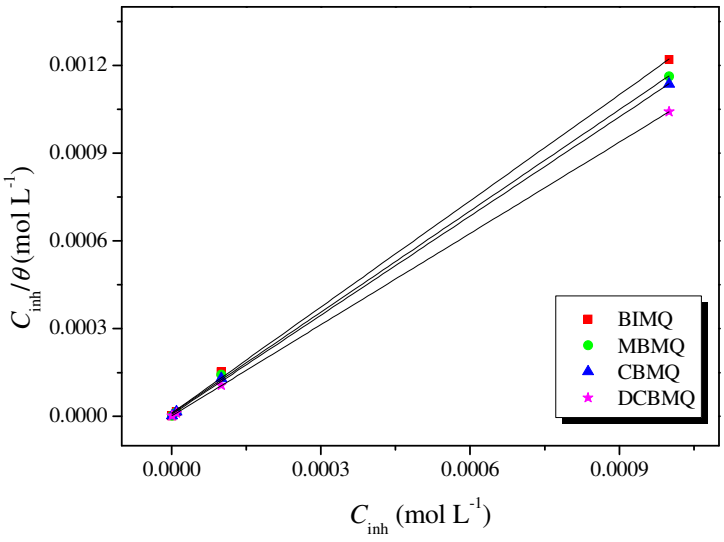

Fig. 10. Langmuir isotherm adsorption model of various synthesized 8-hydroxyquinoline derivatives on the CS surface in 2 M H_3PO_4.

From the intercepts of the straight lines C_{inh}/θ-axis, the K_{ads} values were determined and given in Table 6. The great values of K_{ads} are usually interpreted as an indicator of the adsorption strength between the inhibitor molecules and the CS surface [78]. The calculated ΔG°_{ads} values, using Eq. 16, were also listed in Table 6. The discrimination among chemisorption and physisorption depends on the estimated value of ΔG°_{ads}. For a physisorption mechanism the ΔG°_{ads} of adsorption ought to be equal to or under 20 kJ mol^{-1} while, for chemisorption it is equivalent to or superior to 40 kJ mol^{-1} [79-81]. According to these informations, the obtained ΔG°_{ads} values indicate that the adsorption mechanism of 8-hydroxyquinoline derivatives on CS surface in phosphoric electrolyte is typical of chemisorption. The negative value of DCBMQ indicates its strong adsorption on the CS surface [82,83]. Moreover, $|\Delta G^{\circ}_{ads}|$ of 8-hydroxyquinoline derivatives decreases in the order DCBMQ > CBMQ > MBMQ > BIMQ, this is in great concurrence with the ranking of inhibitive properties got from the electrochemical methods.

Table 6
Thermodynamic parameters for the adsorption of various synthesized 8-hydroxyquinoline derivatives in 2 M H_3PO_4 on the CS at 303 K.

Inhibitor	R^2	K_{ads} (10^4 M^{-1})	ΔG°_{ads} (kJ mol^{-1})	$-Q_{ads}$ (kJ mol^{-1})	ΔS°_{ads} (kJ mol^{-1})
BIMQ	0.999	9.08	-38.88	-7.64	103.10
MBMQ	0.999	10.07	-39.14	-7.55	104.26
CBMQ	0.999	14.47	-40.05	-11.89	92.94
DCBMQ	1.000	76.25	-44.24	-25.35	62.34

The estimation of the adsorption heat ($-Q_{ads}$) was assessed from the next equation [84,85]:

$$\left(\frac{\theta}{1-\theta}\right) = qC_{inh}\left(\frac{-Q_{ads}}{RT}\right) \quad (17)$$

where q is a constant, C_{inh} is the inhibitor concentration, θ is the occupied, (1 - θ) is the vacant site not occupied by the inhibitor [86]. Fig. 11. illustrates the variation of Ln [θ/(1 - θ)]

as a function of the inverse of the temperature for the different synthesized compounds. The lines obtained have a slope equal to ($-Q_{ads}/R$). The negative values of $-Q_{ads}$, given in Table 6, indicated that the adsorption of used inhibitors on the CS surface is exothermic. In other words, the negative $-Q_{ads}$ values exhibit that the rate of adsorption and the inhibition efficiency decreased with increase in temperature also supporting physical adsorption [87]. It is reported that the adsorption heat might be approximately considered as the standard enthalpy of adsorption (ΔH^{o}_{ads}) under studied conditions [60,88]. Therefore, the standard adsorption entropy (ΔS^{o}_{ads}) was obtained based on following thermodynamic basic equation [87,88]:

$$\Delta G^{o}_{ads} = \Delta H^{o}_{ads} - T\,\Delta S^{o}_{ads} \quad (18)$$

The obtained ΔS^{o}_{ads} values in the presence of studied compounds are huge and positive (Table 6), uncovers that a decline in disordering during the passage of from reactant to the activated complex [89].

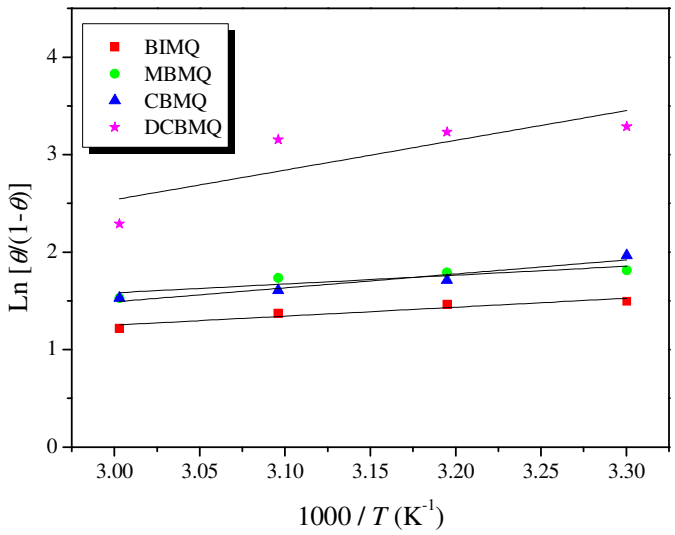

Fig. 11. Ln (θ/(1- θ)) vs. 1/T for adsorption of synthesized 8-hydroxyquinoline derivatives on the CS surface.

X-ray photoelectron spectroscopy (XPS) analysis was performed to provide insight to the adsorption mechanism of the 8-hydroxyquinoline derivatives and to investigate the composition of the organic adsorbed layer on the CS surface in the phosphoric acid medium. High-resolution XPS spectra (C 1s, N 1s, O 1s, Cl 2p, P 2p and Fe 2p), obtained from carbon-steel sample subsequent of immersion in 2 M H_3PO_4 with 10^{-3} M of inhibitor at 303 K are shown in Fig. 12. Only XPS results of DCBMQ are presented. XPS spectra show complex forms, which were assigned to the corresponding species through a deconvolution fitting procedure using the CASA XPS software.

The deconvolution of the C 1s spectrum may be fitted into four components, indicating different carbon environments, located at 285.0, 286.0, 288.8 and 290.2 eV (Fig. 12, Table 7). The first component, has the largest contribution (61 %), can be assigned to the C–C, C=C and C–H bonds in the DCBMQ molecule [90]. The second constituent is mainly ascribed to the C–N, C=N and C-O bonds [91]. The third component can be associated to the carbon atom of the $C=N^+$ in 8-quinolinol and in benzimidazole moieties in the DCBMQ molecule [92], resulting probably from the protonation of the =N– structure, as described in the Scheme 2, and/or the coordination of nitrogen with the iron of steel surface. The last and less intense component (2 %) at binding energy (290.2 eV) can be ascribed to shake-up satellite due to π–π^* transitions in aromatic rings [93].

The high-resolution Cl 2p core-level of CS substrate covered with DCMBQ is best resolved with at least two spin–orbit-split doublets (Cl $2p_{1/2}$ and Cl $2p_{3/2}$) as illustrated in Fig. 12, with binding energy for Cl $2p_{3/2}$ peak lying at about 200.5 eV [94]. This component can be associated to Cl–C bond of $Cl_2C_6H_2$ group [94], belonging to the DCMBQ molecule.

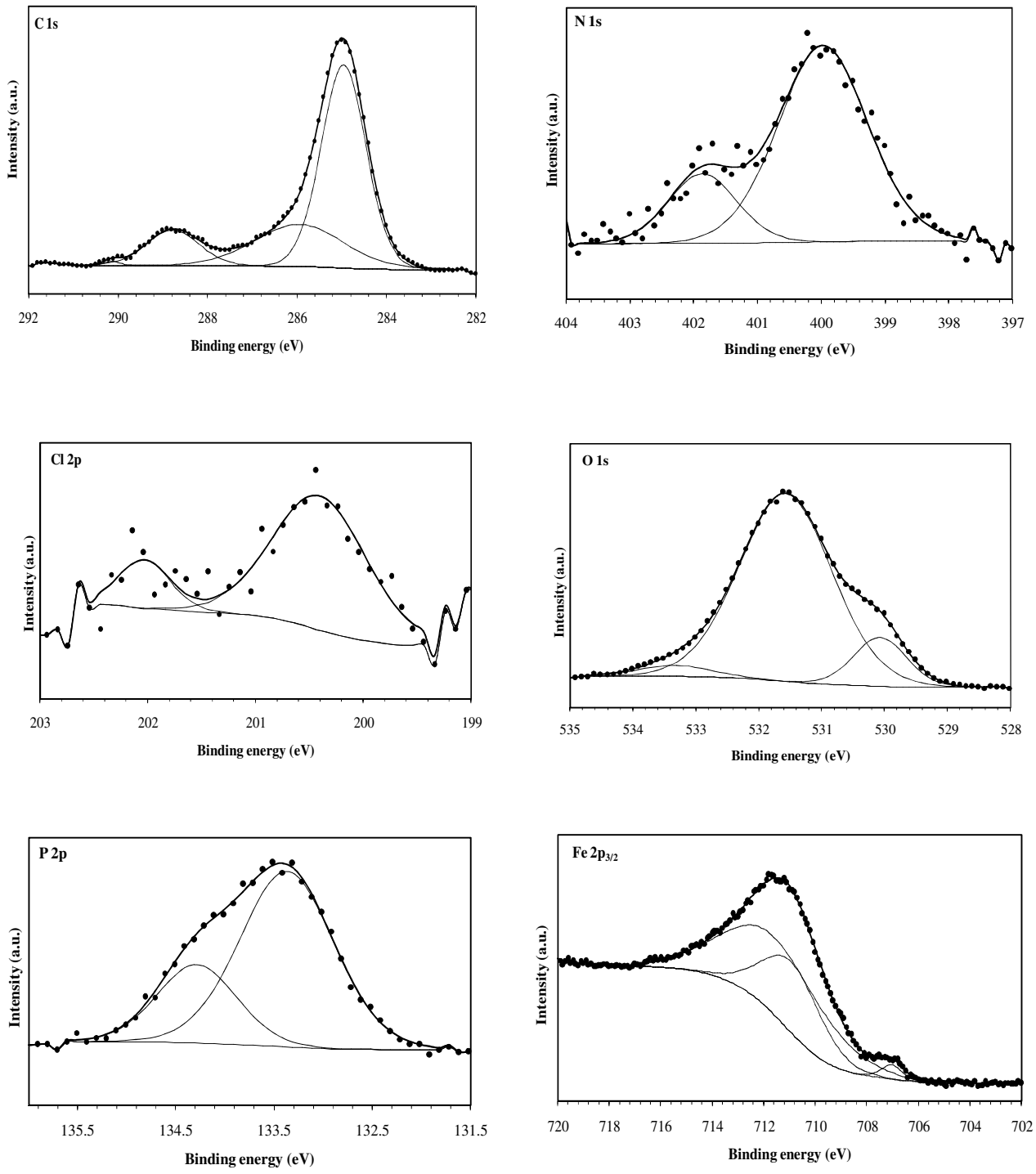

Fig. 12. High-resolution X-ray photoelectron deconvoluted profiles of C 1s, N 1s, Cl 2p, O 1s, P 2p and Fe $2p_{3/2}$ for DCBMQ treated CS substrate.

Table 7

Binding energies (eV), relative intensity and their assignment for the major core lines observed of DCMBQ treated CS substrate

Element	Position (eV)	Assignment
C 1s	285.0 (61 %)	C–H / C–C / C=C
	285.9 (25 %)	C–N / C=N / C–O
	288.8 (12 %)	$C{=}N^{+}$
	290.2 (2 %)	π–π* shakeup satellite
N 1s	400.0 (79 %)	=N– structure, N–C
	401.9 (21 %)	$=N^{+}H$
O 1s	530.1 (12 %)	O^{2-} in Fe_2O_3 / O=P in $FePO_4$
	531.6 (84 %)	OH^{-} in FeOOH / (P–O in $FePO_4$) / C–O
	533.3 (4 %)	Adsorbed H_2O
Cl 2p	200.5 (83 %)	Cl–C ($Cl\ 2p_{3/2}$)
	202.0 (17 %)	Cl–C ($Cl\ 2p_{1/2}$
P 2p	133.4 (72 %)	$P\ 2p_{3/2}$ (PO_4^{3-} in $FePO_4$)
	134.3 (28 %)	$P\ 2p_{1/2}$ (PO_4^{3-} in $FePO_4$)
Fe $2p_{3/2}$	707.1 (4 %)	Fe^{0}
	710.9 (33 %)	Fe^{3+} in Fe_2O_3 and in FeOOH
	711.6 (63 %)	Fe^{3+} in FeOOH and in $FePO_4$

The investigated bare CS is nitrogen free [95] and therefore, the adsorption of 8-hydroxyquinoline derivatives on the steel surface can be explained based especially on the N 1s signal presence. The surveyed spectrum for N 1s of protected carbon steel with DCBMQ in 2 M H_3PO_4 can be fitted into two main components indicating therefore the presence of two chemical states of nitrogen (Fig. 12, Table 7). The presence of the N species demonstrates that the investigated 8-hydroxyquinoline derivative (DCMBQ) molecules are adsorbed on the steel surface. Indeed, the first N 1s component, located at 400.0 eV, has the largest contribution (79%) and can be attributed to the C–N in the benzimidazole moiety and to the unprotonated N atom (=N– structure) in the 8-quinolinol and benzimidazole moieties [96]. It is significant that this component slightly shifted to higher binding energy side (ΔE_b = 0.51 eV) compared to that one observed in the case of pure DCMBQ (Fig. 13). The same trend is shown in the case of the other 8-hydroxyquinoline derivatives (Table 8). This behavior was explained by the coordination of the unprotonated N with the iron atom of steel surface, i.e. formation of N-Fe bond complex, which leads to a positive polarization of the nitrogen atom, and therefore a core-level chemical shift to higher binding energy is produced [97,98]. The

second N 1s component, located at 401.9 eV, component may be associated to the positively charged nitrogen, and could be related to protonated nitrogen atoms (=N^+H–) in the 8-quinolinol and benzimidazole moieties in the DCBMQ molecule [99,100]. On the basis on the N 1s XPS results, we can conclude that the adsorption occurs through chemical chelation of the vacant d orbitals of iron with the lone sp^2 electron pairs present on the N atom (=N– structure) in the 8-quinolinol and in benzimidazole moieties of the investigated inhibitors.

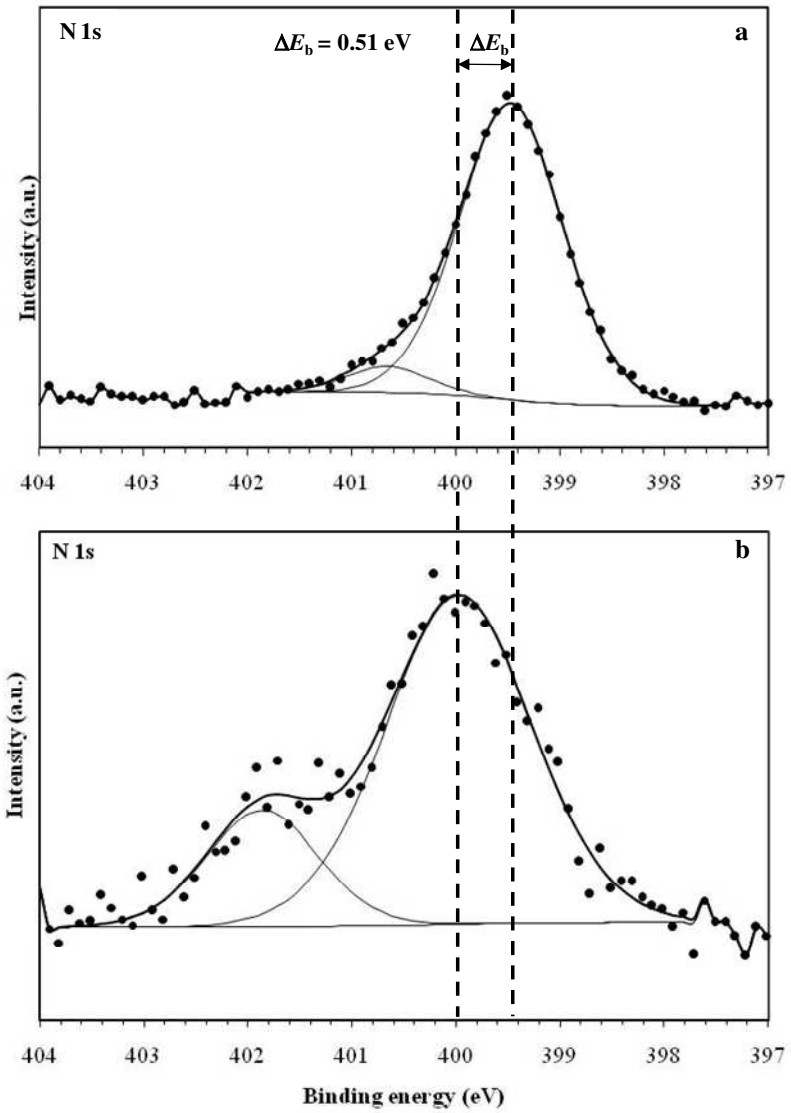

Fig. 13. High-resolution X-ray photoelectron deconvoluted profile of N 1s for a-pure DCBMQ and b- DCBMQ treated CS substrate in 2 M H_3PO_4 medium.

Table 8
Shift binding energy values for N 1s component (=N– structure) of 8-hydroxyquinoline derivatives before and after immersion in 2 M H_3PO_4 medium.

Inhibitor	ΔE_b (eV)
BIMQ	0.70
MBMQ	0.63
CBMQ	0.32
DCBMQ	0.51

The O 1s spectrum for CS surface after immersion in 2 M H_3PO_4 solution containing DCMBQ can be resolved into three components (Fig. 12, Table 7). The first one, at 530.1 eV, is attributed to oxygen double bonded to Fe^{3+} in the iron oxide (Fe_2O_3) [101] and non-bridging oxygen in the phosphate group (P=O) [94]. The second component, located at. 531.6 eV, is the most intense one (80 %), can be assigned to combined effects of singly bonded oxygen (–O–) in Fe–O, in P–O and in C–O–H groups. Indeed, this component can be partly ascribable to OH^- of hydrous iron oxides, such as FeOOH [102] and to O–P in the adsorbed phosphate group (PO_4^{3-}) [103] and partly assigned to singly bonded oxygen (–O–) in C–O and in O–H which are present in the DCMBQ molecules [104]. However, the separation of inorganic (O in FeOOH, phosphates) and organic oxygen (O in carbonyl groups) contributions since O 1s signal is not possible [105]. The latest at 533.3 eV can be attributed to oxygen of adsorbed water [106], which remained on the surface after drying the sample.

The P 2p spectrum of CS surface after immersion in 2 M H_3PO_4 solution containing DCMBQ was fitted into two asymmetric main components ~0.9 eV apart, assigned to P $2p_{3/2}$ at 133.5 eV and P $2p_{1/2}$ at 134.4 eV, due to spin splitting, as given in Fig. 12. This is attributed to PO_4^{3-} in agreement with the presence of the $FePO_4$ as detected in the O 1s spectrum [103].

From the Fe2p signal in Fig. 12 for the CS surface covered with DCMBQ, two characteristic peaks $Fe2p_{1/2}$ at 725 eV (not given) and $Fe2p_{3/2}$ at 711 due to spin splitting are evident. The deconvolution of the high resolution Fe $2p_{3/2}$ XPS spectrum consists in three main components, as shown in Fig. 12 and Table 7, corresponding to the same groups

combining oxygen to iron, observed in the case of the O 1s signal: Fe_2O_3, FeOOH and $FePO_4$. The first one, at 707.1 eV, was attributed to metallic iron [92]. The second one at 710.9 eV may be associated to ferric oxide species such as Fe_2O_3 (i.e., Fe^{3+} oxide) and/or to ferric hydroxide species such as FeOOH [92]. The latest, at 711.6 eV, presents the highest contribution (62 %), can be associated to the presence of FeOOH and $FePO_4$ [92,107].

XPS surface elemental analyses of DCMBQ extract and DCMBQ-treated steel samples were also performed and given in Table 9. In both cases, the sum of the atom concentrations was normalized to 100% in order to easily compare surface concentrations for the different elements. Inspection of the obtained results shows the presence of N atom (3.72 %) on the steel surface probably due to the DCMBQ adsorption through chemical chelation of the lone sp^2 electron pairs present on the N atom of the hetercocyclic ring of 8-hydroxyquinoline derivative with the vacant d orbitals of iron. The atom concentration of oxygen is high in the case of DCMBQ-treated steel sample (38.25 %) compared to that of DCMBQ powder (13.51 %) (Table 8). This difference is normally due to the formation of oxidized species (Fe_2O_3, FeOOH and $FePO_4$) in 2 M H_3PO_4 and therefore DCMBQ molecules are incorporated into the oxide/hydroxide iron layer formed on the CS surface. The appearance of phosphorus element (4.56 %) on the steel surface confirms the formation of $FePO_4$ due to the testing medium (2 M H_3PO_4).

The above XPS detail analyses (qualitative and quantitative) demonstrate that the presence of chemical (chemisorption) interactions between surface steel ions and DCMBQ and confirm the adsorption isotherm findings. The addition of this 8-hydroxyquinoline derivative in the corrosive solution promotes the formation of the stable metal-organic complex (DCMBQ/Fe) and an insoluble oxide layer leading to reduce the attack of acid ions as well as restraining the corrosion process simultaneously.

Table 9
Surface elemental concentrations (% At.) in DCMBQ powder and DCMBQ treated-steel

Element	DCMBQ powder	DCMBQ treated-steel
C	72.66	49.05
O	13.51	38.25
N	7.71	3.72
Fe	—	4.41
P	—	4.56
Cl	6.12	—

3.3. Quantum chemical calculations

DFT/B3LYP/6-31+G(d,p) optimized structures of BIMQ, CBMQ, DCBMQ and MBMQ are shown in Fig. 14. It was observed that the quinolin-8-ol ring and benzimidazole ring are not on the same plane as the two rings have a torsion angle of about 79°–82° depending on the molecule. In other words, there is a need to identify the ring moiety that has the maximum overlap with mild steel in the adsorption process. Though the variation in the dihedral angles (listed in Fig. 14) does not follow a particular trend, it is noteworthy that BIMQ with the largest torsion angle, -81.50° (between the two rings) has the lowest inhibition efficiency, while DCBMQ with the lowest torsion angle, 79.24° has the highest inhibition efficiency recorded from the experiments. This suggests that planarity of the molecules might influence their corrosion inhibition efficiency [108-110].

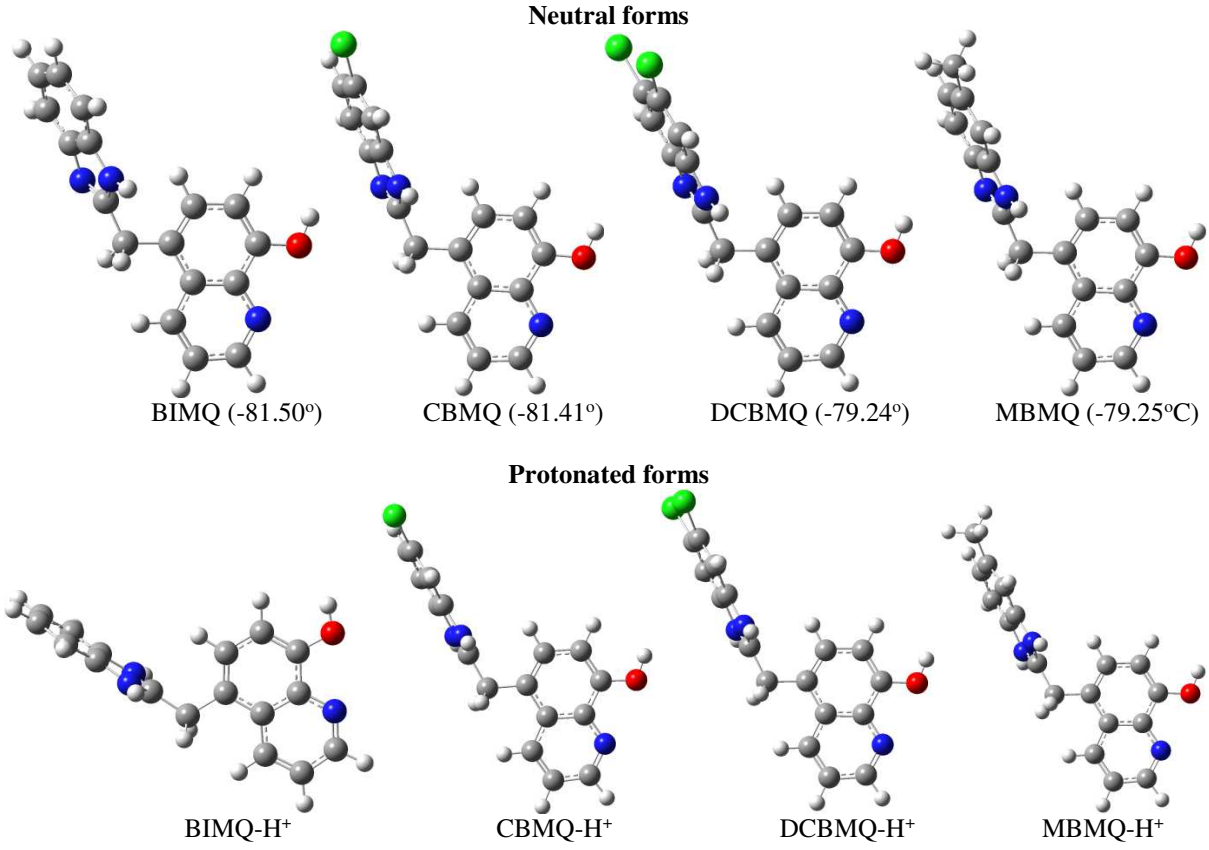

Fig. 14. Optimized structures of the neutral and protonated forms of the studied 8-hydroxyquinoline derivatives.

The frontier molecular orbitals electron density isosurfaces are shown in Fig. 15. The distribution of highest occupied molecular orbital (HOMO) electron density for the molecules revealed that the major orbitals that contribute to the HOMO are those of the quinolin-8-ol moiety. Surprisingly the electron density of the lowest occupied molecular orbitals are also distributed over the quinolin-8-ol ring. These observations could lead one to assume that the inhibitor molecules would preferably interact with mild steel via the quinolin-8-ol. The adsorption of the inhibitor molecules on mild steel surface might be through the plane of quinolin-8-ol ring.

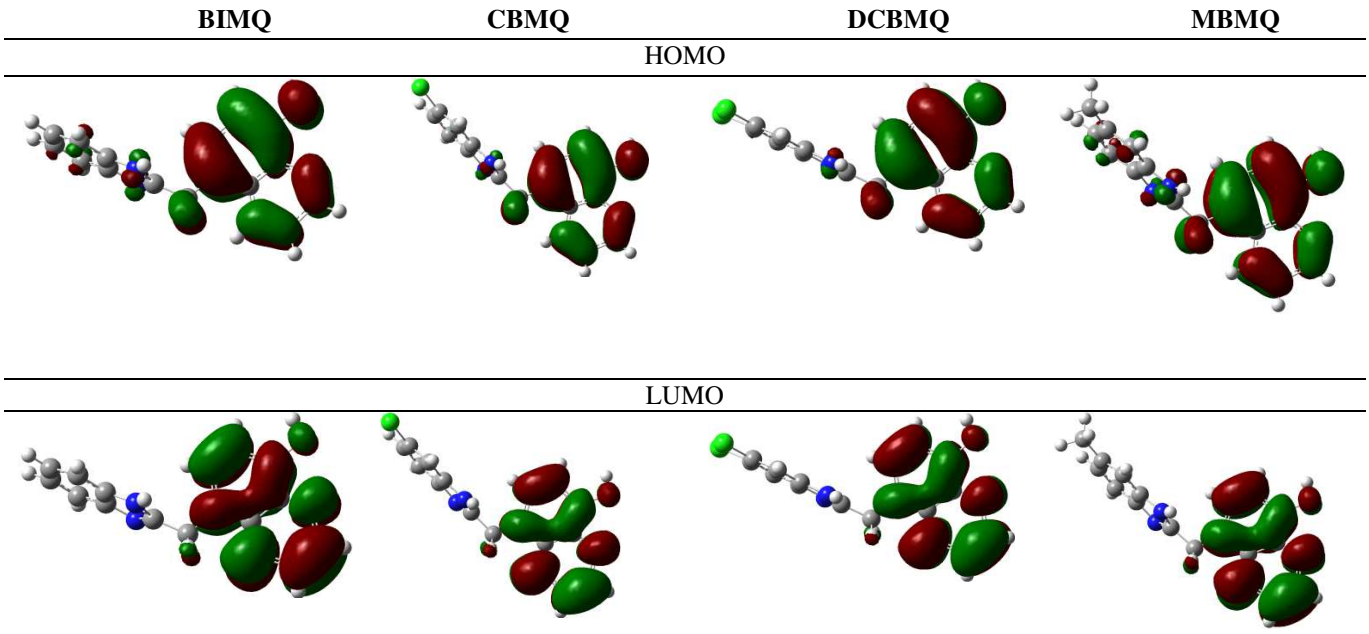

Fig. 15. HOMO and LUMO electron density isosurfaces of the investigated 8-hydroxyquinoline derivatives (isosurfave value = 0.02).

Selected quantum chemical parameters or reactivity indices of the studied inhibitor molecules (both neutral and protonated) are listed in Table 10. The studied compounds are more prone to protonation on the sp^2 benzimizalole nitrogen since benzimidazole is more basic (having a smaller pK_b) than quinoline [111]. Therefore, the protonated species were considered as those in which the proton is attached to the benzimidazole sp^2 nitrogen. For a conventional corrosion inhibitor whose reactivity is governed by its frontier molecular orbitals behavior, higher HOMO energy (E_{HOMO}) and lower LUMO energy (E_{LUMO}) are associated with higher tendency to donate electron to vacant metallic orbital, and hence higher corrosion inhibition efficiency [112]. Few instances of lower E_{LUMO} as an indication of possible back-donation from occupied orbitals of the metal to the anti-bonding orbitals of the inhibitor and a drive for improved adsorption of the inhibitor molecules on the metal surface have also been documented [113,114].

The trend of E_{HOMO} values in Table 10 when compared with the order of inhibition efficiencies does not support increasing inhibition efficiency with increasing E_{HOMO}.

However, a near linear correlation was observed for the E_{LUMO} values in comparison with the order of inhibition efficiencies recorded from the experiments (DCBMQ > CBMQ > MBMQ > BIMQ) such that DCBMQ with the lowest E_{LUMO} has the highest inhibition efficiency.

Table 10

Quantum chemical parameters for the neutral and protonated forms of of 8-hydroxyquinoline derivatives obtained using the B3LYP/6-31+G(d,p)//IEFPCM model.

Parameters→ Inhibitor↓	E_{HOMO} (eV)	E_{LUMO} (eV)	ΔE (eV)	η (eV)	χ (eV)	ΔN	Dipole moment (Debye)
Neutral species							
BIMQ	-6.116	-1.835	4.281	2.140	3.975	0.197	5.031
CBMQ	-6.130	-1.842	4.288	2.144	3.986	0.195	3.767
DCBMQ	-6.141	-1.850	4.291	2.145	3.995	0.192	5.309
MBMQ	-6.107	-1.830	4.277	2.139	3.969	0.199	5.218
Protonated species							
IMQ-H^+	-6.319	-1.978	4.341	2.171	4.148	0.155	13.364
CBMQ-H^+	-6.328	-2.288	4.040	2.020	4.308	0.127	8.947
DCBMQ-H^+	-6.338	-2.282	4.055	2.028	4.310	0.126	6.545
MBMQ-H^+	-6.311	-1.972	4.339	2.169	4.142	0.156	12.352

Furthermore, electronegativity is a measure of the ability of a molecule to retain its pairs of electrons. The order of electronegativity of the inhibitors is DCBMQ > CBMQ > MBMQ ≈ BIMQ, which suggests than the corrosion inhibition potentials of the molecules might be related with the tendency of the molecules to accept electrons from occupied metallic orbitals. The dipole moments for the neutral inhibitor molecules do not correlate with the observed trend of inhibition efficiencies. However, the dipole moments for the protonated species suggest that a protonated molecule with lower dipole moment is better disposed to accumulation in the surface layer of the metal and therefore has higher corrosion inhibition efficiency [112,115,116].

3.4. Monte Carlo simulations

Adsorption of the studied inhibitor molecules on mild steel surface was modelled in the absence and presence of phosphoric acid ions. The equilibirium configurations for the adsorption the molecules on Fe(110) both in isolation and in the presence of 60 H_3O^+ and 20 PO_4^{3-} are shown in Fig. 16. It is evident from BIMQ/Fe(110), CBMQ/Fe(110), DCBMQ/Fe(110) and MBMQ/Fe(110) that the inhibitor molecules adsorb on Fe(110) surface via the plane of the quinolin-8-ol moiety as the plane of the ring lies nearly flat to the metallic surface. Since the inhibitor molecules would compete with acidic ions (H_3O^+ and PO_4^{3-}), the adsorption of inhibitor molecules in the presence of these ions was also examined and the equilibirium configurations in Fig. 16 revealed that the studied inhibitor molecules have good tendency of displacing the corrosive acidic ions from the metallic surface. Adsorption energies of the optimized inhibitor-Fe(110) complexes without and with acidic ions are listed in Table 11. The order of increasing magnitude of the adsorption energy (E_{ads}) for the adsorption of isolated inhibitor molecule (in the absence of corrosive acidic ions) is DCBMQ (E_{ads} = -666.99 kJ/mol) > CBMQ (E_{ads} = -646.24 kJ/mol) > MBMQ (E_{ads} = -642/77 kJ/mol) > BIMQ (E_{ads} = -621.11 kJ/mol). Similar trend was obtained for the adsorption of inhibitor molecules in the presence of acidic ions. The simulation results are in good agreeement with the experimentally observed trend of corrosion inhibition efficiencies.

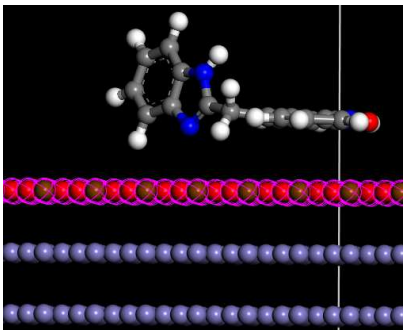

BIMQ/Fe(110)

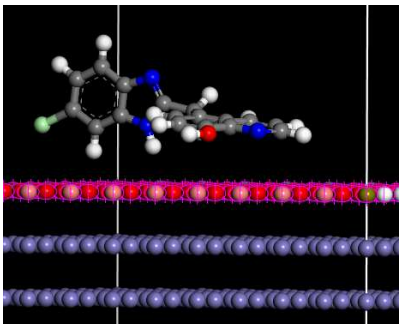

CBMQ/Fe(110)

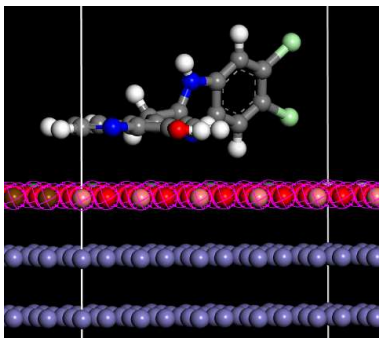

DCBMQ/Fe(110)

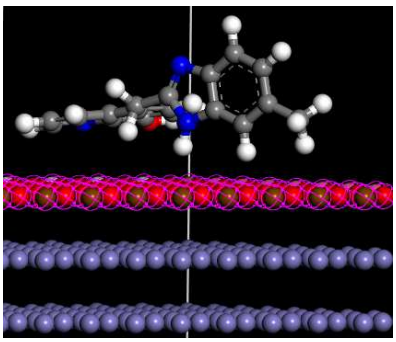

MBMQ/Fe(110)

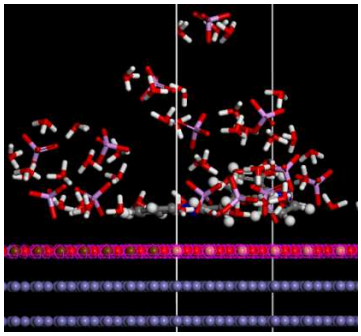

BIMQ + 60 H_3O^+ + 20 PO_4^{3-}/Fe(110)

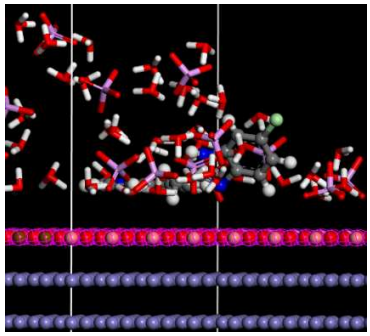

CBMQ + 60 H_3O^+ + 20 PO_4^{3-}/Fe(110)

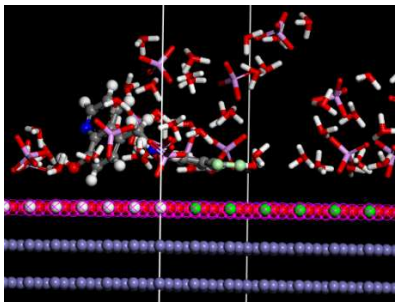

DCBMQ + 60 H_3O^+ + 20 PO_4^{3-}/Fe(110)

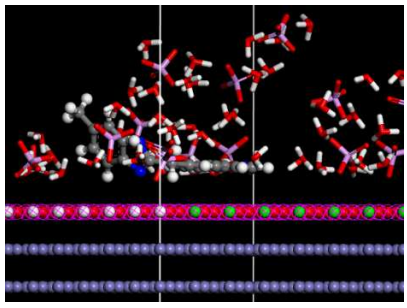

MBMQ + 60 H_3O^+ + 20 PO_4^{3-}/Fe(110)

Fig. 16. Adsorbed inhibitor molecules on Fe(110) surface in absence and presence of 60 molecules of H_3O^+ and 20 molecules of PO_4^{3-} obtained from Monte Carlo simulation.

Table 11

Estimated energy values for the adsorption of 8-hydroxyquinoline derivatives on Fe(110) surface in the absence and presence of 60 molecules of H_3O^+ and 20 molecules of PO_4^{3-} obtained from Monte Carlo simulation.

System	E_{ads} (kJ/mol)
BIMQ/Fe(110)	-621.11
CBMQ/Fe(110)	-646.24
DCBMQ/Fe(110)	-666.99
MBMQ/Fe(110)	-642.77
BIMQ + 60 H_3O^+ + 20 PO_4^{3-}/Fe(110)	-775.38
CBMQ + 60 H_3O^+ + 20 PO_4^{3-}/Fe(110)	-856.85
DCBMQ + 60 H_3O^+ + 20 PO_4^{3-}/Fe(110)	-831.08
MBMQ + 60 H_3O^+ + 20 PO_4^{3-}/Fe(110)	-808.74

4. Conclusions

Four new the 8-ydroxyquinoline derivatives containing benzimidazole moiety were synthesized and identified by ^{1}H, ^{13}C NMR and elemental analysis. The impact of these four heterocyclic compounds on the corrosion inhibition for carbon steel in 2 M H_3PO_4 solution was investigated using experimental and theoretical techniques. The experimental results showed that the chemical structure of the 8-ydroxyquinoline derivatives containing benzimidazole moiety impairs the inhibitory efficiency, generally they are good to excellent protection for steel corrosion. At the concentrations studied, inhibition performance follows the sequence DCBMQ > CBMQ > MBMQ > BIMQ. The results obtained from potentiodynamic polarization data indicate that the investigated compounds are mixed type inhibitors. Impedance studies were analysed using an equivalent circuit for effects of concentration and temperature for all tested inhibitors. All 8-ydroxyquinoline derivatives are adsorbed on the metal surface according to Langmuir adsorption isotherm model and the corresponding values of ΔG^{o}_{ads} revealed that their adsorption mechanism on steel surface is mainly due to chemisorption. XPS results confirm the thermodynamic findings and reveal the formation of protective film on the carbon steel surface in 2 M H_3PO_4 medium, composed by an iron oxide/hydroxide/phosphates layer, in which the 8-hydroxyquinoline molecules are incorporated. Both the computational DFT calculations and Monte Carlo simulations results revealed that the inhibitor molecules adsorb on mild steel surface through the 8-hydroxyquinoline ring plane and the theoretical parameters correlate reasonably with the trend of experimental inhibition efficiencies.

Conflicts of interest

The authors declare no conflicts of interest.

References

[1] M. El Faydy, F. Benhiba, B. Lakhrissi, M. Ebn Touhami, I. Warad, F. Bentiss, A. Zarrouk, J. Mol. Liq. 295 (2019) 111629.

[2] D.S. Chauhan, M.A. Quraishi, A.A. Sorour, S.K. Saha, P. Banerjee, RSC Adv. 9 (2019) 14990–15003.

[3] W. Guo, S. Chen, Y. Feng, C. Yang, J. Phys. Chem. C 111 (2007) 3109–3115.

[4] N.O. Eddy, E.E. Ebenso, Afr. J. Pure Appl. Chem. 2 (2008) 107–115.

[5] M. El Faydy, M.Galai, R. Touir, A. El Assyry, Touhami, B. Lakhrissi, A. Zarrouk, J. Mater. Environ. Sci. 7 (2016) 1406–1416

[6] I.B. Obot, S.A. Umoren, N.O. Obi-Egbedi, Int. J. Electrochem. Sci. 7 (2012) 10215–10232.

[7] H. Zarrok, S. S. Al-Deyab, A. Zarrouk, R. Salghi, B. Hammouti, H. Oudda, M. Bouachrine, F. Bentiss, Int. J. Electrochem. Sci. 7 (2012) 4047–4063.

[8] A. Zarrouk, B. Hammouti, H. Zarrok, M. Bouachrine, K.F. Khaled, S.S. Al-Deyab, T.B. Hadda, Int. J. Electrochem. Sci. 6(2012) 6353–6364.

[9] H. Zarrok, K. Al Mamari, A. Zarrouk, R. Salghi, B. Hammouti, S. S. Al-Deyab, E. M. Essassi, F. Bentiss, H. Oudda, Int. J. Electrochem. Sci. 7 (2012) 10338–10357.

[10] A.K. Singh, M.A. Quraishi, Mater. Chem. Phys. 123 (2010) 666–677.

[11] M. El Faydy, M. Galai, A. El Assyry, A. Tazouti, R. Touir, B. Lakhrissi, M. Ebn Touhami, A. Zarrouk, J. Mol. Liq. 219 (2016) 396–404.

[12] A.K. Singh, B. Chugh, S.K. Saha, P. Banerjee, E.E. Ebenso, S. Thakur, B. Pani, Results. Phys. 14 (2019) 102383.

[13] H. Zarrok, H. Oudda, A. El Midaoui, A. Zarrouk, B. Hammouti, M. Ebn Touhami, A. Attayibat, S. Radi, R. Touzani, Res. Chem. Intermediat. 38 (2012) 2051–2063.

[14] A. Ghazoui, A. Zarrouk, N. Bencaht, R. Salghi, M. Assouag, M. El Hezzat, A. Guenbour, B. Hammouti, J. Chem. Pharm. Res. 6 (2014) 704–712.

[15] H. Zarrok, A. Zarrouk, R. Salghi, H. Oudda, B. Hammouti, M. Assouag, M. Taleb, M. Ebn Touhami, M. Bouachrine, S. Boukhris, J. Chem. Pharm. Res. 4 (2012) 5056–5066.

[16] M.A. Hegazy, M. Abdallah, M.K. Awad, M. Rezk, Corros. Sci. 81 (2014) 54–64.

[17] M.H.M. Hussein, M.F. El-Hady, H.A.H. Shehata, M.A. Hegazy, H.H.H. Hefni, J. Surfactants Deterg. 16 (2013) 233–242.

[18] V.V. Torres, R.S. Amado, C.F. de Sá, T.L. Fernandez, C.A.S. Riehl, A.G. Torres, E. D'Elia, Corros. Sci. 53 (2011) 2385–2392.

[19] M.A. Hegazy, A.M. Badawi, S.S. Abd El Rehim, W.M. Kamel, Corros. Sci. 69 (2013) 110–122.

[20] I.B. Obot, N.O. Obi-Egbedi, Curr. Appl. Phys. 11 (2011) 382–392.

[21] M.E. Belghiti, Y. Karzazi, A. Dafali, I.B. Obot, E.E. Ebenso, K.M. Emran, I. Bahadur, B.Hammouti, F. Bentiss, J. Mol. Liq. 216 (2016) 874–886.

[22] H. About, M. El Faydy, F. Benhiba, Z. Rouifi, M. Boudalia, A. Guenbour, H. Zarrok, B. Lakhrissi, H. Oudda, I. Warad, A. Zarrouk, J. Bio. Tribo. Corros. 5 (2019) 50

[23] X.H. Li, S.D. Deng, H. Fu, Corros. Sci. 53 (2011) 3704–3711.

[24] X.H. Li, S.D. Deng, H. Fu, Corros. Sci. 53 (2011) 664–670.

[25] H. Zarrok, A. Zarrouk, R. Salghi, B. Hammouti, M. Elbakri, M. Ebn Touhami, F. Bentiss, H. Oudda, Res. Chem. Intermediat. 40 (2014) 801–815.

[26] Y.J. Yang, Y.K. Li, L. Wang, H. Liu, D.M. Lu, L. Peng, Int. J. Electrochem. Sci. 14 (2019) 3375–3392.

[27] EG. Ebrahimi, J. Neshati, F. Rezaei, Prog .Org. Coat. 105 (2017) 1–8.

[28] T. Poornima, J. A. Nayak, N. Shetty, Corros. Sci. 53 (2011) 3688–3696.

[29] M. Benabdellah, R. Touzani, A. Dafali, B. Hammouti, S. El Kadiri, Mater. Lett. 61 (2007) 1197–1204.

[30] D. Ben Hmamou, A. Zarrouk, R. Salghi, H. Zarrok, Eno E. Ebenso, B. Hammouti, M.M. Kabanda, N. Benchat, O. Benali, Int. J. Electrochem. Sci. 9 (2014) 120–138.

[31] D. Ben Hmamou, R. Salghi, A. Zarrouk, H. Zarrok, B. Hammouti, S. S. Al-Deyab, A. El Assyry, N. Benchat, M. Bouachrine, Int. J. Electrochem. Sci. 8 (2013) 11526–11545.

[32] M. Belayachi, H. Serrar, H. Zarrok, A. El Assyry, A. Zarrouk, H. Oudda, S. Boukhris, B. Hammouti, Eno E. Ebenso, A. Geunbour, Int. J. Electrochem. Sci. 10 (2015) 3010–3025.

[33] M.A. Hegazy, J. Mol. Liq. 208 (2015) 227–236.
[34] R.S. Keri, S.A. Patil, Biomed. Pharmacother. 68 (2014) 1161–1175
[35] P. Singh, V. Srivastava, M.A. Quraishi, J. Mol. Liq. 216 (2016) 164–173.
[36] W. Zhang, R. Ma, H. Liu, Y. Liu, S. Li, L. Niu, J. Mol. Liq. 222 (2016) 671–679.
[36] N. Du, Q. Mei, M. Lu, Synthetic Met. 149 (2005) 193–197.
[38] B. Himmi, S. Kitane, A. Eddaif, J. Joly, F. Hlimi, F. Soufiaoui, M. Bahloul, A. Sebban, J. Heterocyclic. Chem. 45 (2008) 1023–1026.
[39] V. D.Warner, J. N. Sane, D. B. Mirth, S. S. Turesky, B. Soloway, J. Med. Chem. 19 (1976) 167–169.
[40] M. Tourabi, K. Nohair, M. Traisnel, C. Jama, F. Bentiss, Corros. Sci. 75 (2013) 123–133.
[41] D.A. Shirley, Phys. Rev. B 5 (1972) 4709–4714.
[42] A.D. Becke, J. Chem. Phys 98 (1993) 5648–5652.
[43] A. D. Becke, Phys. Rev. A 38 (1988) 3098–3100.
[44] C. Lee, W. Yang, R.G. Parr, Phys. Rev. B 37 (1988) 785–789.
[45] J.H. Christensen, A.J. Smith, R.B. Reed, K.L. Elmore, J. Chem. Eng. Data 11(1966) 60–63.
[46] H.P.R. Frederiske, Dielectric measurements, in: T.F. Connolly (Ed.), Electr. Prop. Solids, first ed., Plenum Press, London, 1972, pp. 85–147.
[47] K.O. Sulaiman, A.T. Onawole, Comput. Theor. Chem. 1093 (2016) 73–80.
[48] M.J. Frisch, G.W. Trucks, H.B. Schlegel, G.E. Scuseria, M.A. Robb, J.R. Cheeseman, G. Scalmani, V. Barone, B. Mennucci, G.A. Petersson, et al. Gaussian 09, Revision D.01; Gaussian, Inc.: Wallingford CT, 2009.
[49] M. El Faydy, R. Touir, M. Ebn Touhami, A. Zarrouk, C. Jama, B. Lakhrissi, L. O. Olasunkanmi, E. E. Ebenso, F. Bentiss, Phys. Chem. Chem. Phys. 20 (2018) 20167–20187.
[50] A. Kokalj, Chem. Phys. 393 (2012) 1–12.
[51] H. Lgaz, R. Salghi, I.H. Ali, Int. J. Electrochem. Sci. 13 (2018) 250–264.
[52] R.G. Pearson, Inorg. Chem. 27 (1988) 734–740.
[53] K. Marusic, H.O. Curkovic, H. Takenouti, Electrochim. Acta 56 (2011) 7491–7502.
[54] N.A. Negm, N.G. Kandile, I.A. Aiad, M.A. Mohammad, Colloid. Surface 391 (2011) 224–233.
[55] D.K. Yadav, M.A. Quraishi, B. Maiti, Corros. Sci. 55 (2012) 254–266.
[56] A.A. Hermas, M.S. Morad, M.H. Wahdan, J. Appl. Electrochem. 34 (2004) 95–102.
[57] C.M. Palomar-Pardavé, M. Romero-Romo, H. Herrera-Hernández, M.A. Abreu-Quijano, N.V. Likhanova, J. Uruchurtu, J.M. Juárez-García, Corros. Sci. 54 (2012) 231–243.
[58] S.S. Abdel Rehim, H.H. Hassan, M.A. Amin, Appl. Surf. Sci. 187 (2002) 279–290.
[59] M.A. Amin, S.S.A. El-Rehim, E.E.F. El-Sherbini, R.S. Bayoumi, Electrochim. Acta. 52 (2007) 3588–3600.
[60] A.K. Singh, M.A. Quraishi, Corros. Sci. 52 (2010) 152–160.
[61] R.S. Goncalves, D.S. Azambuja, A.M. Serpa Lucho, Corros. Sci. 44 (2002) 467–479.
[62] D.S. Chauhan, K.R. Ansari, A.A. Sorour, M.A. Quraishi, H. Lgaz, R. Salghi, Int. J. Biol. Macromol. 107 (2018) 1747–1757.
[63] M. Abdallah, M.A. Hegazy, M. Alfakeer, H. Ahmed, Green. Chem. Lett. Rev. 11(2018) 457–468.
[64] R. Macdonald, D.R. Franceschetti, in: J.R. Macdonald (Ed.), Impedance Spectroscopy, Wiley, New York, 1987, p. 96.
[65] D.A. Lopez, S.N. Simison, S.R. de Sanchez, Acta 48 (2003) 845–854.
[66] S. Martinez, M. Metikoš-Huković, J. Appl. Electrochemi. 33 (2003) 1137–1142.
[67] N. Labjar, M. Lebrini, F. Bentiss, N.E. Chihib, S. El Hajjaji, C. Jama, Mater. Chem. Phys. 119 (2010) 330–336.
[68] M. El Faydy, B. Lakhrissi, A. Guenbour, S. Kaya, F. Bentiss, I. Warad, A. Zarrouk, J. Mol. Liq. 280 (2019) 341–359.
[69] B. Chugha, A.K. Singh, S. Thakura, B. Panic, A.K. Pandeya, H. Lgaz, I.M. Chungd, E.E. Ebenso, J. Phys. Chem. C (2019) 22897–22917.
[70] M. El Faydy, M. Rbaa, L. Lakhrissi, B. Lakhrissi, I. Warad, A. Zarrouk, I. B. Obot, Surf. Interf. 14 (2019) 222–237.
[71] T. Szauer, A. Brandt., Electrochim. Acta 26 (1981) 1253–1256.
[72] A. Popova, M. Christov, A. Zwetanova, Corros. Sci. 49 (2007) 2131–2143.
[73] A. Popova, E. Sokolova, S. Raicheva, M. Chritov, Corros. Sci. 45 (2003) 33–41.

[74] C. Verma, A. Singh, G. Pallikonda, M. Chakravarty, M. A. Quraishi, I. Bahadur, E.E. Ebenso, J. Mol. Liq. 209 (2015) 306–319.
[75] D.K. Yadav, M.A. Quraishi, Ind. Eng. Chem. Res. 51 (2012) 14966–14979.
[76] F. Bentiss, M. Bouanis, B. Mernari, M. Traisnel, H. Vezin, M. Lagrenée, Appl. Sur. Sci. 253 (2007) 3696–3704.
[77] A.K. Singh, S. Thakur, B. Pani, E.E. Ebenso, M. A. Quraishi, A.K. Pandey, ACS Omega 3 (2018) 4695–4705.
[78] R. K. Gupta, M. Malviya, K.R. Ansari, H. Lgaz, D.S.Chauhan, M.A. Quraishi, Mater. Chem. Phys. 236 (2019) 121727.
[79] F. Bentiss, M. Traisnel, H. Vezin, H.F. Hildebrand, M. Lagrenée, Corros. Sci. 46 (2004) 2781–2792.
[80] F. Bentiss, M. Lebrini, M. Lagrenée, M. Traisnel, A. Elfarouk, H. Vezin, Electrochim. Acta 52(2007) 6865–6872.
[81] I. Lukovits, A. Shaban, E. Kalman, Electrochim. Acta 50 (2005) 4128–4133.
[82] A. K. Singh, S. Thakur, B. Pani, G. Singh, New J. Chem. 42 (2018) 2113–2124.
[83] M. El Faydy, M. Galai, M.E. Touhami, I.B. Obot, B. Lakhrissi, A. Zarrouk, J. Mol. Liq. 248 (2017) 1014–1027.
[84] F.H.M. Azahar, S. Mitra, A. Yabushita, A. Harata, B.B. Saha, K. Thu, Appl. Therm. Eng. 143 (2018) 688–700.
[85] E.E. Oguzie, V.O. Njoku, C.K. Enenebeaku, C.O. Akalezi, C. Obi, Corros. Sci. 50 (2008) 3480-3486.
[86] E. A. Noor, A. H. Al-Moubaraki, Mater. Chem. Phys. 110 (2008) 145–154.
[87] G. Avci, Colloid Surface A, 317 (2008), 730-736.
[88] S.M.A. Hosseini, A. Azimi, Corros. Sci. 51(2009), 728–732.
[89] M. Sahin, S. Bilgic, H. Yılmaz, Appl. Surf. Sci. 195 (2002) 1–7.
[90] D. Briggs and M.P. Seah, Practical Surface Analysis by Auger and X-ray Photoelectron Spectroscopy, John Wiley & Sons Ltd., Sussex, 1983 (Section 9.4 and Appendix 2).
[91] H. Ouici, M. Tourabi, O. Benali, C. Selles, C. Jama, A. Zarrouk, F. Bentiss, J. Electroanal. Chem. 803 (2017) 125–134.
[92] M. Bouanis, M. Tourabi, A. Nyassi, A. Zarrouk, C. Jama, F. Bentiss, Appl. Surf. Sci. 389 (2016) 952–966.
[93] A.M. Puziya, O.I. Poddubnaya, R.P. Socha, J. Gurgul, M. Wisniewski, Carbon 46 (2008) 2113–2123.
[94] F. Moulder, W.F. Stickle, P.E. Sobol, K.D. Bomben, in: J. Chastain (Ed.), Handbook of X-Ray Photoelectron Spectroscopy, Perkin-Elmer Corp., Minnesota, USA, 1992.
[85] F.Z. Bouanis, F. Bentiss, S. Bellayer, M. Traisnel, J.B. Vogt, C. Jama, Mater. Chem. Phys. 127 (2011) 329–334.
[96] O. Olivares, N.V. Likhanova, B. Gómez, J. Navarrete, M.E. Llanos-Serrano, E.Arce, J.M. Hallen, Appl. Surf. Sci. 252 (2006) 2894–2909.
[97] O. Olivares, N.V. Likhanova, B. Gómez, J. Navarrete, M.E. Llanos-Serrano, E. Arce, J.M. Hallen, Appl. Surf. Sci. 252 (2006) 2894–2909.
[98] Y. Kharbach, F.Z. Qachchachi, A. Haoudi, M. Tourabi, A. Zarrouk, C. Jama, L.O. Olasunkanmi, E.E. Ebenso, F. Bentiss, J. Mol. Liq. 246 (2017) 302–316.
[99] G.A. Schick, Z.Q. Sun, Spectroscopic characterization of sulfonyl chloride immobilization on silica, Langmuir 10 (1994) 3105–3110.
[100] N. El Hamdani, R. Fdil, M. Tourabi, C. Jama, F. Bentiss, Appl. Surf. Sci. 357 (2015) 1294–1305.
[101] P. Bommersbach, C. Alemany-Dumont, J.P. Millet, B. Normand, Electrochim. Acta 51 (2005) 1076–1084.
[102] W. Temesghen, P.M.A. Sherwood, Anal. Bioanal. Chem., 2002, 373, 601–608.
[103] X. Wu, K. Gong, G. Zhao, W. Lou, X. Wang, W Liu, RSC Adv. 8 (2018) 4595-4603.
[104] A.G. Kannan, N.R. Choudhury, N.K. Dutta, Polymer, 48 (2007) 7078–7086.
[105] A.R. González-Elipe, A. Martínez-Alonso, J.M.D. Tascón, Surf. Interface Anal. 12 (1988) 565–571.

[106] K. Babić-Samardžija, C. Lupu, N. Hackerman, A.R. Barron, A. Luttge, Langmuir 21 (2005) 12187–12196.
[107] G. Gunasekaran, L.R. Chauhan, Electrochim. Acta 49 (2004) 4387–4395.
[108] C. Verma, M. A. Quraishi, L. O. Olasunkanmi, Eno E. Ebenso, RSC Adv. 5 (2015) 85417–85430.
[109] E. E. Ebenso, M. M. Kabanda, L. C. Murulana, A. K. Singh, S. K. Shukla, Ind. Eng. Chem. Res., 51 (2012) 12940–12958.
[110] F. Bentiss, M. Lagrenée, J. Mater. Environ. Sci. 2(2011) 13–17.
[111] D.M Smith, G. Tennant, Benzimidazoles and Cogeneric Tricyclic Compounds, Part 1 edited by P. N. Preston with contributions by John Wiley & Sons, New York, 1981. P. 582.
[112] L.O. Olasunkanmi, I.B. Obot, M.M. Kabanda, E.E. Ebenso, J. Phys. Chem. C 119 (2015) 16004−16019.
[113] Y. Karzazi, M. El Alaoui Belghiti, A. Dafali, B. Hammouti, J. Chem. Pharm. Res. 6 (2014) 689−696.
[114] K. Barouni, A. Kassale, A. Albourine, O. Jbara, B. Hammouti, L. Bazzi, J. Mater. Environ. Sci. 5 (2014) 456−463.
[115] N. Soltani, M. Behpour, E.E. Oguzie, M. Mahluji, M.A. Ghasemzadeh, RSC Adv. 5 (2015) 11145−11162.
[116] A. Popova, M. Christov, T. Deligeorigiev, Corrosion 59 (2003) 756−764.